

## New parton distributions for collider physics

Hung-Liang Lai,<sup>1,2</sup> M. Guzzi,<sup>3</sup> Joey Huston,<sup>1</sup> Zhao Li,<sup>1</sup>  
 Pavel M. Nadolsky,<sup>3</sup> Jon Pumplin,<sup>1</sup> and C.-P. Yuan<sup>1\*</sup>

<sup>1</sup>*Department of Physics and Astronomy,  
 Michigan State University, East Lansing, MI 48824-1116, U.S.A.*

<sup>2</sup>*Taipei Municipal University of Education, Taipei, Taiwan*

<sup>3</sup>*Department of Physics, Southern Methodist University, Dallas, TX 75275-0175, U.S.A.*

(Dated: March 3, 2019)

### Abstract

We extract new parton distribution functions (PDFs) of the proton by global analysis of hard scattering data in the framework of general-mass perturbative Quantum Chromodynamics. Our analysis includes new theoretical developments together with most recent collider data from deep-inelastic scattering, vector boson production, and single-inclusive jet production, as compared to the previous CTEQ6.6 work. Due to the difficulty in fitting both the DØ Run-II  $W$  lepton asymmetry data and some fixed-target DIS data, we present two families of PDFs, CT10 and CT10W, without and with these high-luminosity  $W$  lepton asymmetry data included in global analysis, to explore possible solutions. With these PDFs, we study theoretical predictions and uncertainties for a diverse selection of processes at the Fermilab Tevatron and the CERN Large Hadron Collider.

arXiv:1007.2241v1 [hep-ph] 14 Jul 2010

---

\*yuan@pa.msu.edu

## Contents

<b>1. Introduction</b>	<b>3</b>
<b>2. New theoretical developments</b>	<b>4</b>
<b>3. New data sets</b>	<b>6</b>
<b>4. Impact of the combined HERA-1 data</b>	<b>7</b>
<b>5. New PDFs without using <math>D\bar{O}</math> Run-II WLasy: CT10</b>	<b>11</b>
<b>6. New PDFs including <math>D\bar{O}</math> Run-II WLasy: CT10W</b>	<b>13</b>
<b>7. Quality of fits to the individual data sets</b>	<b>15</b>
<b>8. Applications to Tevatron and LHC Physics</b>	<b>18</b>
8.1. $W$ and $Z$ Physics	19
8.2. Other Significant Processes	28
8.3. Dijet Invariant Mass Distributions	30
<b>9. Conclusions</b>	<b>32</b>
<b>A. Agreement of QCD theory with the combined HERA-1 data</b>	<b>33</b>
<b>References</b>	<b>35</b>

## 1. INTRODUCTION

Parton distribution functions (PDFs) of the proton are essential for making physical predictions, and potentially extracting revolutionary physics results, from experiments at high energy colliders, such as the Fermilab Tevatron and CERN Large Hadron Collider (LHC). Faithful determination of PDFs and their corresponding uncertainties from global analysis is therefore crucial. There have been continuous efforts in this front by several groups [1–5]. In this paper, we introduce a number of improvements to the theoretical treatment that was used to produce the previous CTEQ6.6 and CT09 PDFs; and also include some important additions to the data sets upon which the determination is based. We begin by summarizing the principal changes in theoretical treatment.

First, we now treat the systematic error that corresponds to an overall normalization factor in each of many data sets in the same manner that all other systematic error parameters are handled: since  $\chi^2$  is a quadratic function of such parameters, the best-fit value can be computed algebraically for any given values of the other fitting parameters. This simplifies the fitting procedure, because the normalizations no longer introduce additional fitting parameters that have to be searched on numerically; and it improves the estimate of uncertainties—expanding them slightly by correctly allowing the normalization estimates to vary along each eigenvector direction during the process of finding the most extreme acceptable fits along each such direction.

Second, we now compute  $\chi^2$ , which measures the consistency between a given set of PDFs and the data, using weight 1 for all experiments (with just one exception to be discussed below). In previous CTEQ fits, weights larger than 1 were applied to some data sets to keep them from being fit badly—especially in the course of defining eigenvector PDF sets that delimit the uncertainty. That goal is now handled instead by adding an extra contribution to the total  $\chi^2$  based on the quality of fit to each individual data set, which halts the displacement along any given eigenvector early if necessary to prevent one or more individual data sets from being too badly described.

Third, we use somewhat more flexible parametrizations for the PDFs at our chosen starting scale  $\mu = 1.3 \text{ GeV}$ , to reduce the error from parametrization dependence. This is especially true in the parametrizations of strange quark and gluon distributions where the constraints from data are still limited. In total, we have 26 free parameters, expanded from 22 used in the CTEQ6.6 analysis.

In addition to the improvements in theoretical treatment, we include here several updates to the input data that are used to determine the PDFs. Recall that in the determination of CT09 PDFs [2], we have included the Tevatron Run-II inclusive jet data constraining the gluon parton distribution function at large momentum fraction  $x$ . Here, we also include additional recent data from HERA and Tevatron experiments. First, we use the recent HERA “combined” data set [3], which was developed by a collaboration between the H1 and ZEUS experiments to replace the original independent data sets from HERA-1. Second, we include data on the rapidity distribution of  $Z^0$  production, which has been measured at the Tevatron by both CDF and DØ collaborations. Finally, we consider data from the Tevatron Run-II  $W$  lepton asymmetry (WLasy) data: the asymmetry in the rapidity distribution of the charged lepton from  $W$  boson decay. These data are sensitive to flavor content in the proton—especially to the ratio of down- and up-quark PDFs:  $d(x)/u(x)$ .

The WLasy data play a special role in this study, because they are found to display considerable tension with respect to some of the previous data sets; and they also show some tension among themselves. Because of this, we present results from two different PDF fits: CT10, in which the high luminosity DØ WLasy data are ignored; and CT10W, in which the DØ WLasy data are instead emphasized by assigning weights on the order of 2–5 to them, which is sufficient to force an acceptable fit to these data sets.

Another aspect of this paper consists of a study of the quality of the fit to the various data sets examined in the global PDF fit. This study aims to quantify the degree of consistency of constraints imposed on the PDFs by different sets of experiments; it is important for understanding the extent of the PDF uncertainty allowed by the current experimental measurements. Similar questions have been addressed recently by the examination of  $\chi^2$  contributions provided by the individual experiments [2, 6], using techniques discussed in Refs. [7, 8]. Here we explore them with the help of the Fisher’s difference function  $S_n$  [9], defined as  $S_n = \sqrt{2\chi_N^2} - \sqrt{2N - 1}$ . This function is convenient for comparing the goodness-of-fit among data sets that contain different numbers of data points  $N$ . With its help, we demonstrate that non-negligible tensions between the fitted data sets (also noticed in Ref. [8]) persist regardless of the number of PDF parameters introduced in the global fit.

The organization of the paper is as follows: Sec. 2 describes the improvements in theoretical treatment; Sec. 3 describes the newly included data sets; Sec. 4 describes the impact of combined HERA-1 data; Sec. 5 describes the PDF fits that omit the new DØ WLasy data; Sec. 6 describes the PDF fits that include that data; Sec. 7 discusses the quality of the fits to each data set; Sec. 8 discusses applications of the new PDFs to collider physics; and Sec. 9 contains our conclusions.

## 2. NEW THEORETICAL DEVELOPMENTS

We have made a number of improvements to the global analysis, as compared to CTEQ6.6 [10] and CT09 [2].

One of the improvements is that the normalization uncertainty in each experiment is handled just like any other systematic error parameter: the dependence of  $\chi^2$  is a quadratic function of the normalization, so the normalization choice that minimizes  $\chi^2$  can be determined algebraically. This simplifies the fitting procedure, because it eliminates the need to assign an explicit (MINUIT [11]) search parameter to describe each normalization factor during the numerical minimization procedure. At the same time, this update improves the estimate of PDF uncertainties by correctly allowing the normalization factors to vary as the dependence of the total  $\chi^2$  on distance along each eigenvector direction is evaluated to determine uncertainty limits. In previous CTEQ analysis, the normalizations were frozen during that exploration, so this upgrade results in a small increase in the final estimated uncertainty range. (We have checked that the normalization shifts found in the fits, both for the central fit and the eigenvector uncertainty sets, lie within a reasonable range as compared to the published normalization uncertainty of each data set.)

To reduce the effect of parametrization dependence, somewhat more flexible parametrizations were used for the parton distributions at our chosen starting scale  $\mu_0 = 1.3 \text{ GeV}$  for DGLAP evolution [12–14], compared to what was used in CTEQ6.6. In all, CT10 makes

use of 26 free parameters (52 eigenvector sets) compared to 22 parameters (44 eigenvector sets) for CTEQ6.6.

In detail, both CT10 and CTEQ6.6 use the same form for  $u_v(x) = u(x) - \bar{u}(x)$ :

$$u_v(x) = a_0 x^{a_1} (1-x)^{a_2} \exp(a_3 x + a_4 x^2 + a_5 \sqrt{x}) \quad (1)$$

For  $d_v(x) = d(x) - \bar{d}(x)$ , the same form is used in CT10, while  $a_5$  was set to 0 in CTEQ6.6, giving CT10 somewhat more freedom. (The coefficients  $a_2, \dots, a_5$  for  $u_v(x)$  and  $d_v(x)$  are taken to be independent, while the  $a_1$  values are assumed to be equal to each other based on expectations from Regge theory.)

For the gluon, CTEQ6.6 also used the form (1) with  $a_5 = 0$ . The same was used in CT10, except that an additional factor  $\exp(-a_6 x^{-a_7})$  was included to allow extra freedom of the gluon at small  $x$ . This extra term is not required from the current data for getting the best fit, since it results in reducing  $\chi^2$  by only 6 units; however, it allows us to better explore the uncertainty in the small- $x$  region, where the data provide little constraint.

For strangeness, CTEQ6.6 used an *ad hoc* parametrization designed to avoid fits in which the strangeness ratio  $(s(x) + \bar{s}(x))/(\bar{u}(x) + \bar{d}(x))$  was counterintuitively large at small  $x$ . In CT10, this has been replaced by the much more flexible form (1) with  $a_4 = 0$ . The desire to impose reasonable expectations on the strangeness ratio is handled in CT10 by adding a soft constraint based on the strangeness ratio at several specific values of  $x$ . (The same power-law behavior was assumed for  $\bar{u}(x)$ ,  $\bar{d}(x)$ , and  $\bar{s}(x)$  in the limit  $x \rightarrow 0$ , based on Regge theory; with the same coefficient for  $\bar{u}$  and  $\bar{d}$ , so that  $\bar{u}(x)/\bar{d}(x) \rightarrow 1$  and  $\bar{s}(x)/\bar{d}(x) \rightarrow \text{const}$  as  $x \rightarrow 0$ .) For simplicity, the symmetric strangeness assumption  $s(x) = \bar{s}(x)$  is made, similar to CTEQ6.6.

When computing the  $\chi^2$  measure of consistency between the PDFs and the data in CT10, we follow the usual CTEQ analysis approach [15, 16] of requiring agreement at the confidence level (CL) of about 90% with each experiment included in the fit, for each final PDF eigenvector set provided to compute the PDF uncertainty. This is achieved, on average, by defining an upper bound on the excursion of the global  $\chi^2$  from its minimal value, chosen so as to keep the  $\chi^2$  function of each individual experiment within the 90% CL computed (for the number of data points in this experiment [17]). In addition to this overall tolerance condition, CTEQ6.6 and the earlier fits assigned weights greater than 1 to some data sets—particularly those with a small number of points—to ensure that the fits to those data sets remained acceptable for all of the eigenvector sets that define the uncertainty range. The procedure for the choice of weights was time-consuming and varied depending on the selection of experiments and “tensions” between them. It could give some experiments with extra weights an undue influence on the best fit.

In the CT10 fit, we introduce a different approach, which reaches the same objective of enforcing the 90% CL agreement with all experiments in a more efficient way. Each data set is assigned weight 1 in CT10, with the exception of the new DØ Run-II WLasy data to be discussed below. Recall the Fisher’s difference function  $S_n$  [9], defined as

$$S_n = \sqrt{2\chi_n^2} - \sqrt{2N_n - 1} \quad (2)$$

for data set  $n$  with  $N_n$  data points. On statistical grounds, this variable is expected to be well approximated by a standard normal distribution (with a mean of zero, variance of 1, and no skewness), independently of the number of points  $N_n$  for  $N_n > 10$ . (See Sec. 7.)

Thus, in an ideal situation, it is easy to assign a confidence level to each excursion of  $S_n$  from its central value, for all practical  $N_n$ . For example, a 90% CL excursion would correspond to  $S_n \approx 1.3$ , cf. Fig. 13.

In reality, the distribution of  $S_n$  values is broader than a Gaussian with variance of unity even in the best fit (cf. Sec. 6), due to imperfect compatibility between the different hadronic scattering data sets. For this reason, in the experiments that have  $\chi_n^2 > N_n$  already in the best fit, we compute  $S_n$  by dividing the  $\chi^2$  value by its best-fit value, to bring the  $S_n$  distribution in close agreement with the standard normal distribution. We then add a penalty term to the log-likelihood function  $\chi^2$  (which also includes the usual  $\chi^2$  term (4) contributed by the individual data points) to exclude solutions with highly improbable positive  $S_n$  for some experiments. Specifically, to find the eigenvector sets of the error PDFs, we add a penalty<sup>1</sup> generated by the cost function

$$P = \sum_n S_n^k \Theta(S_n) \quad (3)$$

to evaluate the overall  $\chi^2$  of a fit, which warrants that none of the alternative eigenvector PDFs can disagree wildly with any individual data set. The theta function  $\Theta(S_n)$  is to indicate that the penalty is applied only for  $S_n$  larger than zero. Because of the rapidly rising power law in Eq. (3), this penalty can quickly shorten the distance to halt the displacement along each eigenvector direction, owing to the overall 90% CL criterion. This guarantees that all data sets are reasonably well described within the estimated PDF uncertainty range. The new procedure captures the idea of preserving 90% CL among data sets [1, 15, 16] explicitly and automatically, while still retains some of the original importance of the usual total  $\chi^2$ .

In particular, we find that the  $S_n$  penalties are important for about half of the final eigenvector sets. The intention of the use of the  $S_n$  factor is to insure that data sets with a small number of data points not be ignored in the global fit; a large increase in the  $\chi^2$  per degree of freedom for this type of data set may result in a relatively small change in the total  $\chi^2$  of the global fit. (The two contributions we included in the effective  $\chi^2$  could be described as analogous to the US congressional system, called Electoral College, where votes in the House are proportional to population—data points in our case—while votes in the Senate represent specific entities—experiments or data sets in our case.)

### 3. NEW DATA SETS

In the past two years, several precise data sets have become available, which expand the scope of earlier data used in the previous CTEQ6.6 [18] and CT09 [19] analyses. This study (CT10 and CT10W, to be more specific below) includes Run-II inclusive jet data from CDF and DØ (included in CT09 analysis, but not in CTEQ6.6), which already agree well with the prediction using CTEQ6.6 PDFs.

The H1 and ZEUS collaborations at the HERA  $ep$  collider released a joint data set

---

<sup>1</sup> In order to ensure the quality of fit to each individual data set at the 90% confidence level,  $k$  is chosen to be 16. The final PDF uncertainty shows little dependence on the exact form of this penalty term, as long as it rises rapidly beyond the 90% confidence level.

[3] that combines results from eleven measurements in neutral-current (NC) and charged-current (CC) deep inelastic scattering (DIS) processes at HERA-1. In previous analyses, when HERA measurements were included as separate data sets, each one was handled independently from the other ten sets, and the correlations between systematic errors in the distinct data sets were neglected. Since many systematic factors are common to the whole HERA experiment and affect all results in a correlated way, Ref. [3] presents the HERA-1 DIS results as a single data set, with all 114 correlated systematic effects shared by each data point. The combined data set has a reduced total systematic uncertainty, as a result of cross calibration of detection parameters between H1 and ZEUS measurements. When the combined HERA-1 data set is used, we observe a reduction in the PDF uncertainty, compared to a counterpart fit based on the separate HERA-1 data sets. We shall defer the detailed discussion on the impact of the combined HERA-1 data in Sec. 4.

New data on the asymmetry in the rapidity distribution of the charged lepton from  $W$  boson decay measured in  $p\bar{p}$  collisions at  $\sqrt{s} = 1.96$  TeV has been published by both CDF [20] and DØ [21, 22] Collaborations. The lower luminosity CDF Run-I and Run-II data agree with all previously available experiments well, whereas high-luminosity DØ Run-II data disagree with some fixed-target DIS experiments badly. Since the DØ Run-II  $W$  lepton asymmetry data (4 data sets with a total of 45 data points) show significant tension with respect to the other data—and to some extent with themselves— we produce two separate fits: CT10, from which the DØ  $W$  electron asymmetry sets are excluded, and CT10W, in which they are included using weight factors larger than 1 to insure an acceptable fit.

Measurements by both CDF and DØ collaborations of the rapidity distribution for  $Z^0$  bosons at the Tevatron are also included in this analysis. The DØ measurement has been shown to agree well with the theory prediction using the existing PDFs, whereas higher luminosity measurement from CDF not as well. When both the DØ Run-II  $W$  lepton asymmetry data and the CDF Run-II  $Z$  rapidity data are included in the fit, the agreement for both becomes better and within our tolerance, although high luminosity CDF  $Z$  rapidity data still exhibits a higher-than-ideal  $\chi^2$  ( $\sim 50$  for 29 data points). We note that the CDF data show a slight preference for CT10W over CT10. The impact of these two data sets on the best fit is quite mild.

In total, the CT10 (CT10W) fit is based on 29 (33) data sets with a total of 2753 (2798) data points. The results of CT10 and CT10W analyses are discussed in sections 5 and 6.

#### 4. IMPACT OF THE COMBINED HERA-1 DATA

The combined H1/ZEUS set on DIS at HERA-1 [3] is included in our analysis together with the estimates of correlated experimental uncertainties provided by HERA experimentalists [23]. When comparing each experimental value  $D_k$  with the respective theory value  $T_k(\{a\})$  (dependent on PDF parameters  $\{a\}$ ), we account for possible systematic shifts in the data, estimated by the correlation matrix  $\beta_{k\alpha}$ . There are  $N_\lambda = 114$  independent sources of experimental systematic uncertainties, quantified by parameters  $\lambda_\alpha$  that should obey the standard normal distribution. The contribution of the combined HERA-1 set to the log-likelihood function  $\chi^2$  is given by

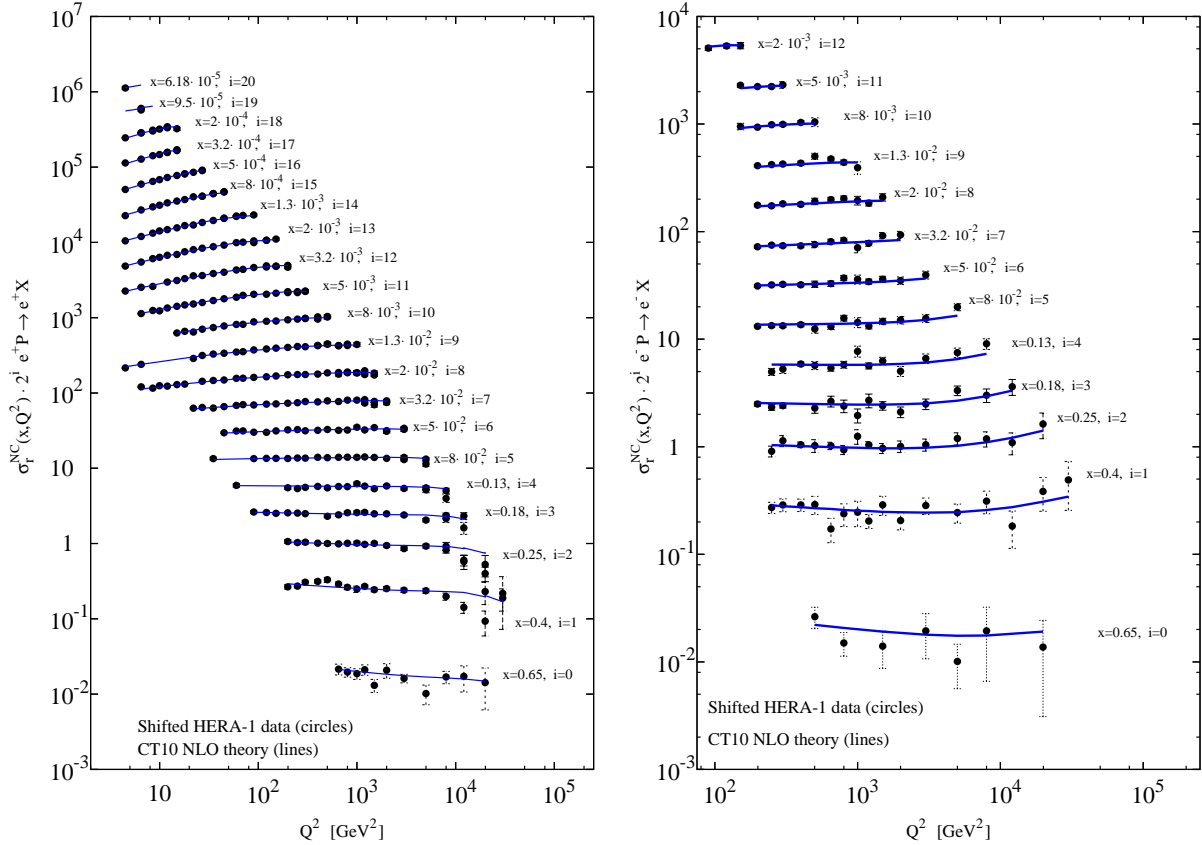


Figure 1: Comparison of CT10 NLO predictions for reduced cross sections in  $e^+p$  (left) and  $e^-p$  (right) neutral-current DIS scattering with the combined HERA data, with correlated systematic shifts included.

$$\chi^2(\{a\}, \{\lambda\}) = \sum_{k=1}^N \frac{1}{s_k^2} \left( D_k - T_k(\{a\}) - \sum_{\alpha=1}^{N_\lambda} \lambda_\alpha \beta_{k\alpha} \right)^2 + \sum_{\alpha=1}^{N_\lambda} \lambda_\alpha^2, \quad (4)$$

where  $N$  is the total number of points,  $s_k = \sqrt{s_{k,\text{stat}}^2 + s_{k,\text{uncor sys}}^2}$  is the total uncorrelated error on the measurement  $D_k$ , obtained by summing the statistical and uncorrelated systematic errors on  $D_k$  in quadrature. Minimization of  $\chi^2$  with respect to the systematic parameters  $\lambda_\alpha$  is realized algebraically, by the procedure explained in Refs. [16, 17].

Both CT10 and CT10W central fits, designated as CT10.00 and CT10W.00 respectively, show good agreement with the combined H1/ZEUS set of reduced DIS cross sections. For the rest of this section, we discuss the CT10 fit; the outcome of the CT10W fit is very similar. We obtain  $\chi^2 \approx 680$  for those  $N = 579$  data points of the combined HERA-1 sample that pass our standard kinematical cuts for the included DIS data,  $Q > 2$  GeV and  $W > 3.5$  GeV. Comparison of theory predictions with the NC  $e^\pm p$  and  $e^-p$  data is shown in Fig. 1. Apart from some excessive scatter of the NC  $e^\pm p$  data around theory predictions, which results in a slightly higher-than-ideal value of  $\chi^2/N = 1.18$ , NLO theory describes well the overall data, without systematic discrepancies.

The data points shown in the figure include systematic shifts bringing theoretical and

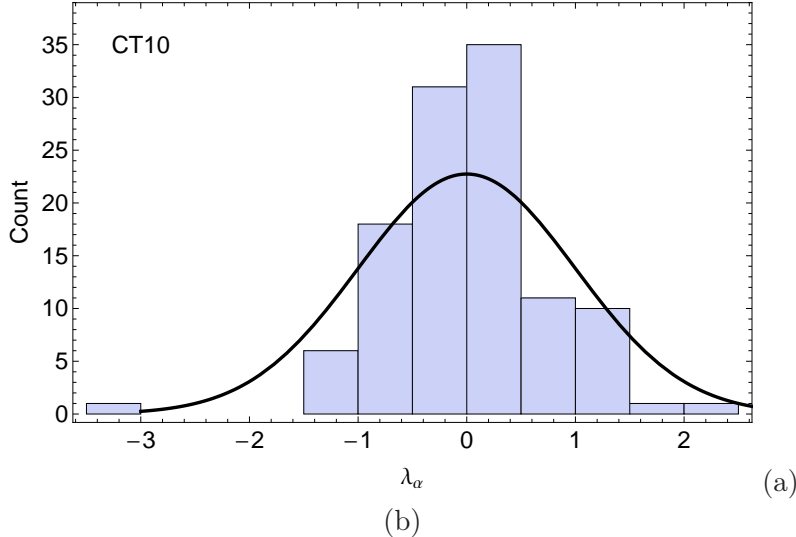


Figure 2: Distribution of systematic parameters  $\lambda_\alpha$  of the combined HERA-1 data set [3] in the CT10 best fit (CT10.00).

experimental values closer to one another, by allowing the systematic parameters  $\lambda_\alpha$  to vary within the bounds allowed by the experimental correlation matrix  $\beta_{k\alpha}$ . As expected, the best-fit values of  $\lambda_\alpha$  are distributed consistently with the standard normal distribution. Their contribution  $\sum_\alpha \lambda_\alpha^2 \approx 65$  to  $\chi^2$  in Eq. 4 is better than the value of 114 expected on statistical grounds.

The histogram of  $\lambda_\alpha$  values obtained in the best CT10 fit (CT10.00) is shown in Fig. 2. The histogram is clearly compatible with its stated Gaussian behavior. In each fit, one observes 1-2 values at  $(\pm)2-3\sigma$ , but those tend to have a large PDF uncertainty (up to  $3\sigma$ ) and are not persistent in all fits.

The overall agreement with the combined HERA-1 data is slightly worse than with the separate data sets, as a consequence of some increase in  $\chi^2/N$  for the NC data at  $x < 0.001$  and  $x > 0.1$ . To elucidate the origin of this increase, we compare the CT10 fit to an alternative fit, in which the combined HERA-1 set is replaced by eleven separate data sets for each HERA DIS measurement, and with the rest of the inputs kept identical to those in the CT10 fit. In the alternative fit, each HERA-1 experiment contributes a  $\chi^2$  term of the same form as in Eq. (4), but with independent correlation matrices  $\beta_{k\alpha}$  and systematic parameters  $\{\lambda_\alpha\}$  in each measurement.

Appendix A examines contributions of individual data points to  $\chi^2$  in the combined and alternative fits and finds them to be consistent with random point-to-point fluctuations of the combined data in the small- $x$  and large- $x$  ranges. The fluctuations are irregular and larger than normally expected, and their spread becomes larger upon the combination of the data sets. At the same time, this analysis does not support systematic differences between the NLO QCD theory and DIS data that could exist if, e.g., the NLO DGLAP evolution were inadequate in the region of small  $x$  and  $Q$  covered by the HERA points [24].

To illustrate modifications induced by the combined HERA-1 set, we compare the CT10 PDFs obtained with this set to those from the alternative fit to eleven separate HERA sets. Figs. 3(a,b) show error bands for (a) the gluon and (b) the charm quark, as a function of

Bjorken  $x$  at  $Q = 2$  GeV. The error bands represent the asymmetric positive and negative uncertainties in the PDFs  $f_a(x, \mu) \equiv f$ , computed as [25]

$$\begin{aligned}\delta^+ f &= \sqrt{\sum_{i=1}^{N_a} \left[ \max \left( f_i^{(+)} - f_0, f_i^{(-)} - f_0, 0 \right) \right]^2}, \\ \delta^- f &= \sqrt{\sum_{i=1}^{N_a} \left[ \max \left( f_0 - f_i^{(+)}, f_0 - f_i^{(-)}, 0 \right) \right]^2},\end{aligned}\tag{5}$$

in terms of  $f_0$ , the best-fit (central) PDF value, and  $f_i^\pm$ , the PDFs for positive and negative variations of the PDF parameters along the  $i$ -th eigenvector direction in the  $N_a$ -dimensional PDF parameter space. In Fig. 3, we compare the uncertainties for the combined HERA set (red solid band) and separate sets (blue hatched band), in which the most pronounced changes are observed in the gluon, charm, and bottom (not shown) distributions. The uncertainties are shown as ratios to the central PDFs in their respective fits,

$$\Delta^{(+)} f(x) = \frac{f_0 + \delta^+ f}{f_0}; \quad \Delta^{(-)} f(x) = \frac{f_0 - \delta^- f}{f_0}.\tag{6}$$

For the other flavors, the changes in the uncertainties are smaller and are not explicitly included. The impact of the HERA-1 data on the uncertainties of the gluon and charm PDFs is quite clear in the small- $x$  region, starting from  $x = 10^{-3}$  and going down to  $x = 10^{-5}$ , where we observe a shrinkage in the error bands. In the large  $x$  region, the error bands for the combined and separate HERA data sets are almost coincident.

Ratios of the central PDFs for each flavor in the CT10 and its alternative (with separate HERA data) fits are shown in Figs. 4(a) and (b), at  $Q = 2$  GeV and 85 GeV. At  $Q = 2$  GeV (Fig. 4(a)) the effect of the new data is again most evident in the behavior of the gluon and charm PDFs at  $x$  below  $10^{-2}$ . These PDFs are suppressed by up to 10% here upon the combination of the HERA sets. In addition, one observes a suppression of the strange (anti-)quark PDF in the best fit of the combined HERA fit, which, however, is small compared to the large PDF uncertainty associated with this flavor. The light-quark PDFs are slightly enhanced at small  $x$  and about the same at medium to large  $x$ .

Fig. 4(b) demonstrates the impact of the DGLAP evolution to  $Q = 85$  GeV on these ratios. Some suppression persists in the gluon PDF at  $x < 0.01$ , but this is washed away by the singlet evolution compared to  $Q = 2$  GeV, which also suppresses the ratios for all quarks in the same  $x$  region. At  $x > 0.1$  the combined HERA data prefer a smaller  $g(x, Q)$  and about the same valence quark PDFs.

All the differences between the PDFs induced by the combined and separate HERA data sets are fully contained in the respective error bands, so no tension between the best-fit solutions of the two fits is observed. The resulting changes in predictions for collider observables, with the exception of those sensitive to gluon or heavy-quark scattering at  $x < 0.01$  and small momentum scales, are thus expected to be mild.

As an illustration, Table I shows percent changes due to the combination of the HERA sets in inclusive  $W$  and  $Z$  boson production cross sections at the Tevatron and LHC, as well as in their ratios, computed at NLO in  $\alpha_s$  in accordance with the settings discussed in Section 8. The largest observed change is an increase of 2.5% in the  $W$  and  $Z$  cross sections

Collider/observable	Change in		
	$\sigma\left(pp^{(-)}(W^{\pm}\rightarrow\ell\nu_{\ell})X\right)$	$\sigma\left(pp^{(-)}\rightarrow(Z^0\rightarrow\ell\bar{\ell})X\right)$	$\frac{\sigma\left(pp^{(-)}(W^{\pm}\rightarrow\ell\nu_{\ell})X\right)}{\sigma\left(pp^{(-)}(Z^0\rightarrow\ell\bar{\ell})X\right)}$
Tevatron, $\sqrt{s} = 1.96$ TeV	+2.6%	+2.5%	-0.05%
LHC, $\sqrt{s} = 7$ TeV	+0.7%	+0.7%	-0.02%
LHC, $\sqrt{s} = 14$ TeV	-0.5%	-0.5%	-0.07%

Table I: Percent changes in CT10 total cross sections for inclusive  $W^{\pm}$  and  $Z^0$  boson production at the Tevatron Run II and LHC, caused by to the replacement of separate HERA-1 cross sections by the combined HERA data set.

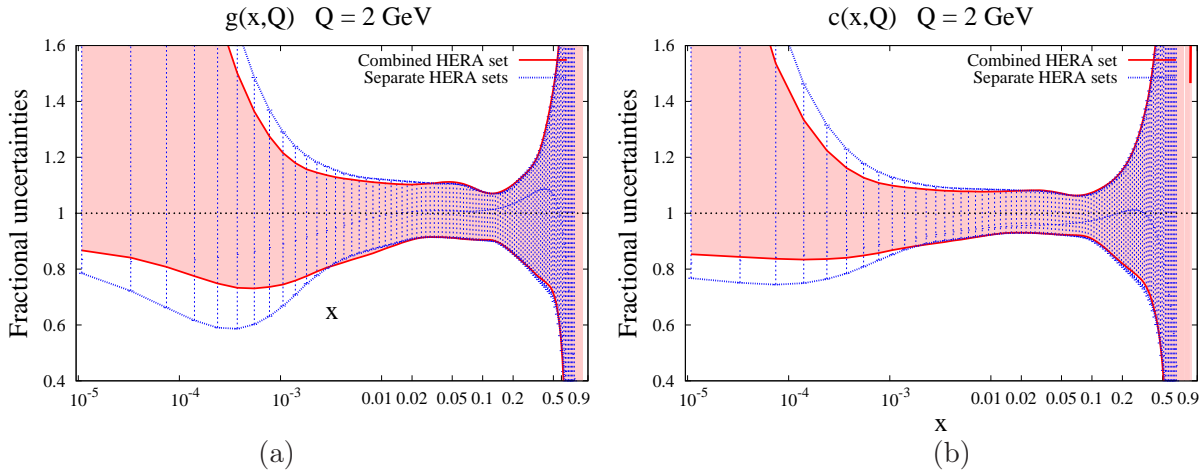


Figure 3: Impact of the new HERA data on the PDFs uncertainties:  $g(x), c(x), Q = 2$  GeV.

in the Tevatron Run II. Changes in the LHC cross sections are positive or negative and are about 0.7% at most. These changes are well correlated in the  $W$  and  $Z$  scattering processes, so that the ratio of the  $W$  and  $Z$  cross sections, shown in the last column of the table, changes (decreases) marginally by 0.02-0.07%.

## 5. NEW PDFS WITHOUT USING DØ RUN-II WLASY: CT10

The CT10 fit makes use of the theoretical improvements discussed in Sec. 2, and the additions to the data set other than DØ Run-II WLasy data discussed in Sec. 3. Note that the lower luminosity CDF Run-II WLasy data [20] have been shown to be in good agreement with CTEQ6.6 predictions, and also included in this analysis.

Figure 5 shows the central fit and uncertainty range of the gluon distribution for CTEQ6.6 and CT10, relative to the CTEQ6.6 best fit. The two are remarkably similar, except at small  $x$ , where parametrization effects are especially important. The uncertainty range is generally *larger* than in CTEQ6.6, in spite of the increased experimental constraints. The additional constraints are offset by the change to weight 1 for every data set, by allowing the experimental normalization factors to vary during eigenvector set searches, and by increased freedom in the parametrizations. (See Sec. 2)

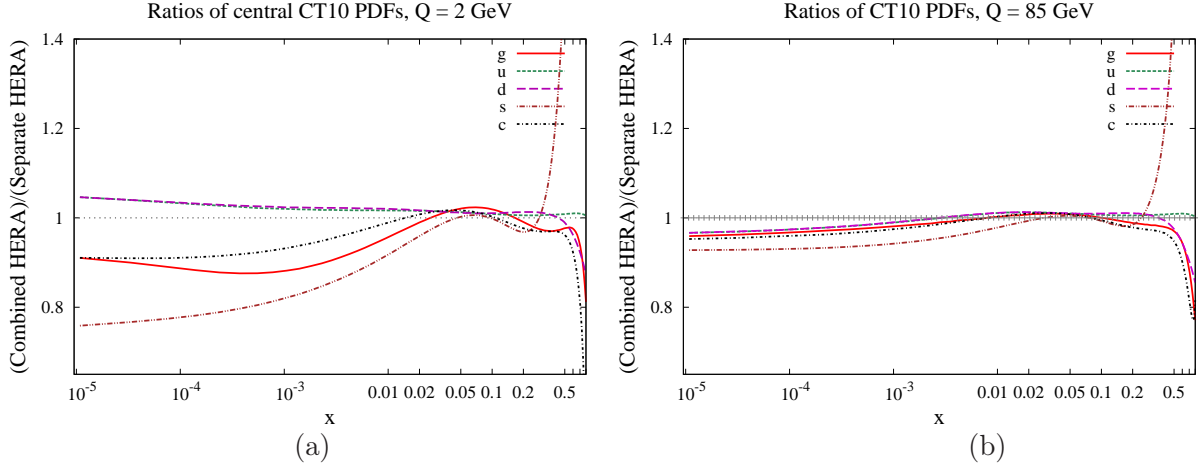


Figure 4: Ratios of CT10 PDFs (fitted to combined HERA data) to the alternative PDFs fitted to separate HERA data for  $Q = 2$  GeV and  $Q = 85$  GeV.

Figures 6 and 7 similarly compare CT10 with CTEQ6.6 for  $u(x)$  and  $d(x)$ . Again CT10 lies within the 90% CL range from CTEQ6.6. However,  $u(x)$  has increased to somewhere close to the CTEQ6.6 estimated upper limit at  $x \sim 0.02$ , even at scale  $\mu = 100$  GeV, again as a result of modifications discussed in in Sec. 2.

Figure 8 compares CT10 with CTEQ6.6 for the strange quark distribution  $s(x) = \bar{s}(x)$ . Here the CT10 central fit again lies well inside the CTEQ6.6 uncertainty estimate; but the CT10 uncertainty on strangeness is much larger than in CTEQ6.6, as a result of its more flexible parametrization assumed in CT10.

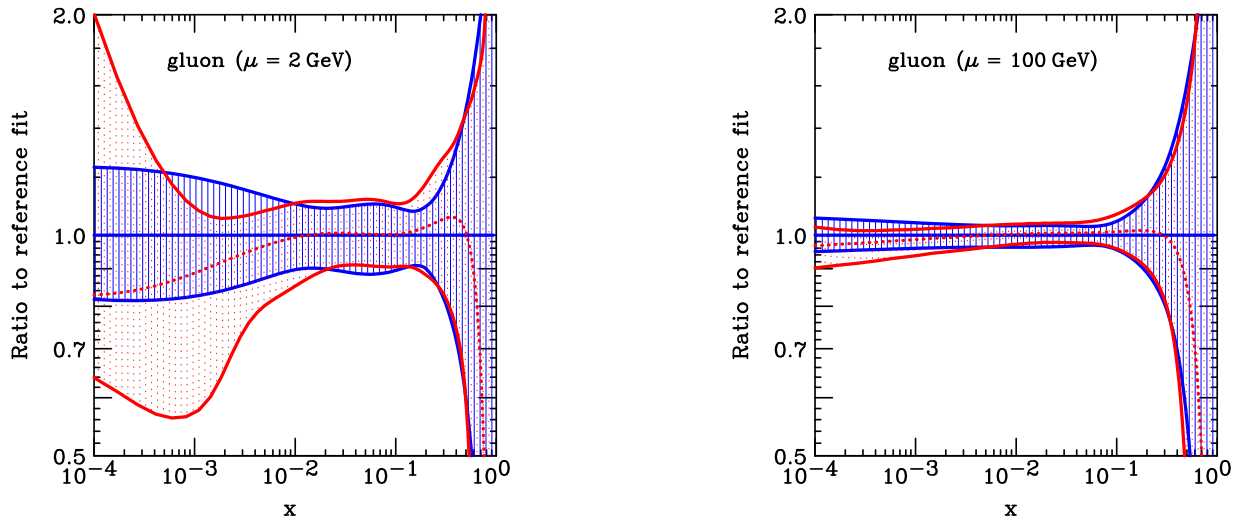


Figure 5: Various PDFs relative to the CTEQ6.6 best fit, for gluon at the scale of 2 GeV and 100 GeV, respectively. Solid curves show the CTEQ6.6 uncertainty and dotted ones for CT10.

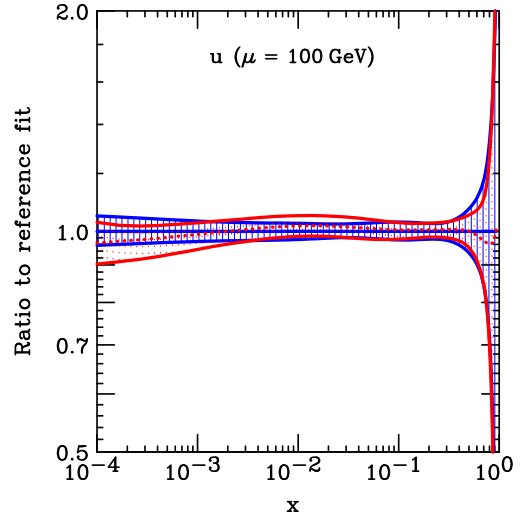
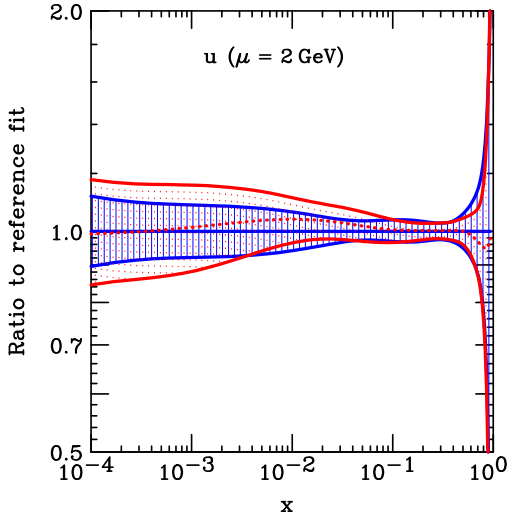


Figure 6: Like Fig. 5, but for  $u$  quark.

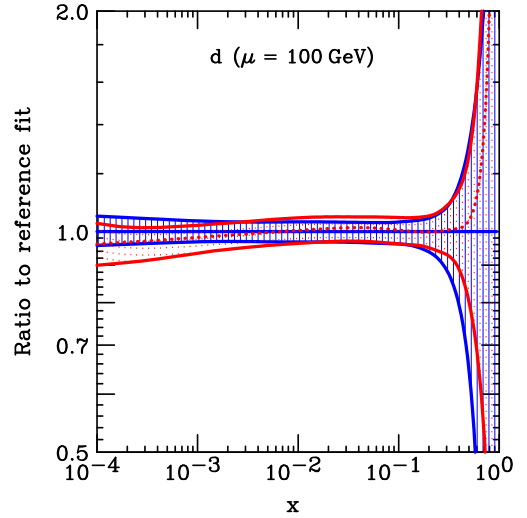
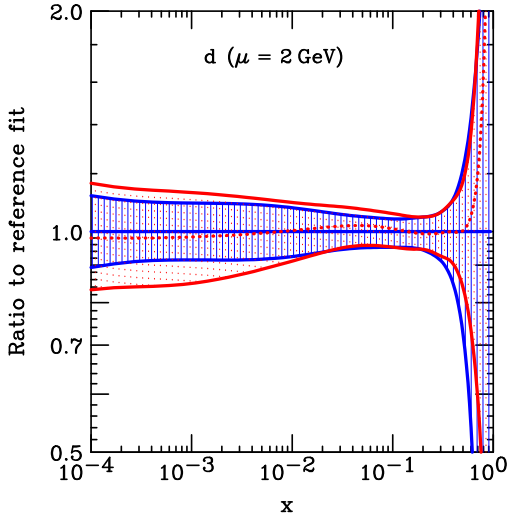


Figure 7: Like Fig. 5, but for  $d$  quark.

## 6. NEW PDFs INCLUDING DØ RUN-II WLASY: CT10W

The new DØ Run-II  $W$  lepton asymmetry data (WLasy) have been shown to disagree with the existing PDFs [21, 22], which include Run-I data in the determination of the CTEQ6.6 and CT09 PDFs. Any fit that does well on Run-II results will have to sacrifice the agreement on Run-I inherently, since both are probing similar PDF region. To accommodate the apparent disagreement of the  $W$  lepton asymmetry data from DØ Run-II, we find it necessary to give the DØ Run-II WLasy data a special emphasis, as we did when high  $E_t$  jets were first included in the global analysis in 1995 [26]. The impact of the weight on  $\chi^2$  for the DØ Run-II WLasy data is documented in Table II.

The table shows that the CT10 best fit, in which the new DØ Run-II WLasy data were not used, disagrees strongly with WLasy1 and WLasy3. The next two columns show the

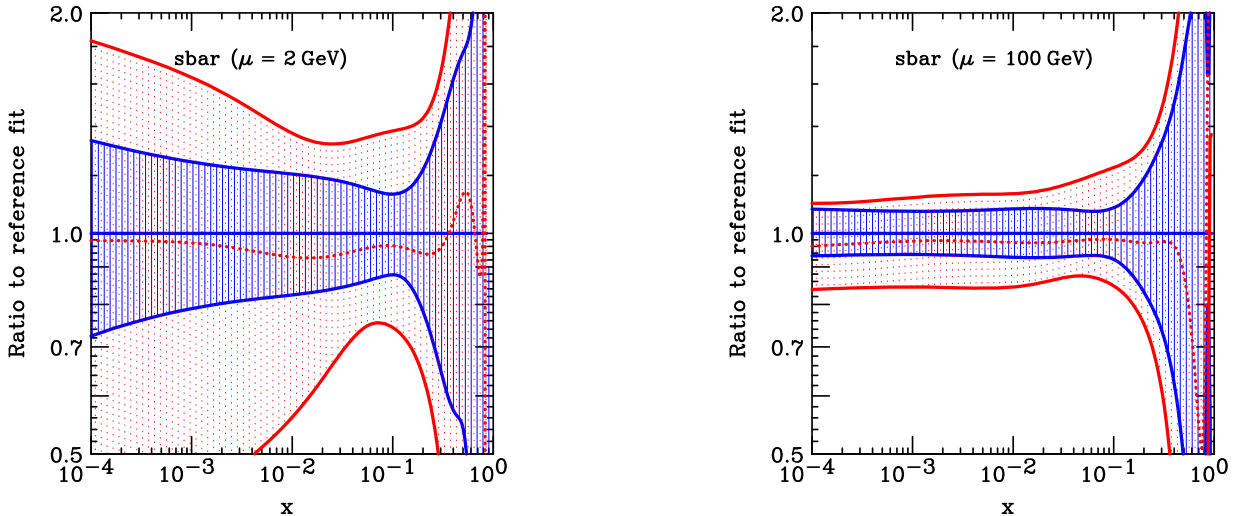


Figure 8: Like Fig. 5, but for  $s = \bar{s}$  quark.

Set	Cut	$N$	$\chi^2$ (CT10)	$\chi^2$ ( $w=1$ )	$\chi^2$ (CT10W)
WLasy1 electron	$P_T > 25$ GeV	12	79.5	37.2	25.3
WLasy2 electron	$25 < P_T < 35$ GeV	12	20.7	20.3	25.5
WLasy3 electron	$P_T > 35$ GeV	12	91.4	41.7	26.5
WLasy4 muon	$P_T > 20$ GeV	9	8.3	10.8	13.5

Table II:  $\chi^2$  of  $D\bar{O}$  Run-II  $W$  lepton asymmetry data, with various weighting factors in the CT10W fits.

effect of including the 4 WLasy sets with weight 1 ( $w = 1$ ). Here, WLasy1 and WLasy3 are still rather poorly fit. This was the motivation for using larger weights (5,2,5,2) to define CT10W. (The missing transverse energy  $\cancel{E}_T$  is required to be larger than 25 GeV in the electron asymmetry data, and 20 GeV in muon data. The number of data points in each data set is denoted as  $N$ .)

Because of the small number of  $D\bar{O}$  WLasy data points, the fit tends to ignore those points where they conflict with other data sets. Hence we define the CT10W best fit by including the four WLasy experiments with weights (5,2,5,2). With this weighting, the fit to the WLasy sets becomes acceptable, although not great.

A measure of the tension between the  $D\bar{O}$  Run-II WLasy data and the CT10 global fit can be obtained by examining the increase in total  $\chi^2$  for the complete data set included in the CT10 analysis when performing the CT10W global analysis. The result is 67, which lies within our estimated 90% probability tolerance, so the CT10W fit can be considered acceptable in the scope of CT10. 54 out of 67 are contributed by NMC  $F_2^D/F_2^P$  ratio data [27] alone. The other major source of conflict comes from the BCDMS deuterium data [28, 29], with an increase of 17 in  $\chi^2$ . Also significantly worse is the fit to the CDF Run-I WLasy data [30], where  $\chi^2$  increases by 5, with only 11 data points. These three sets combined accumulate the extra  $\chi^2$  of 76, already more than 67 the difference between CT10 and CT10W. It shows that the other data sets, in fact, are slightly in favor of CT10W.

The WLasy data sets appear to have considerable tension among themselves also, as can

be seen for example from the fact that the fit to WLasy2 becomes worse than in CT10, even though it is included with a weight of 2 instead of 0, as a result of the weights 5 assigned to WLasy1 and WLasy3.

It is understood that those data sets are the most affected ones since they all provide information on the ratio of  $d/u$  at the overlapping region. Note that nuclear effects could be affecting the data on deuterons [31, 32]. Also, the increase in the total  $\chi^2$  of the non-WLasy data, when comparing the CT10W to CT10 fits, is within our assumed tolerance. Therefore, we conclude that the resulting CT10W we arrive at is a plausible one.

Figures 9–11 show the best fit and uncertainty range for  $g$ ,  $u$ , and  $d$  in CT10 and CT10W. Gluon distributions are more or less the same, both in its central fit and uncertainty range, between CT10 and CT10W. Up quark distribution of CT10W becomes smaller starting at  $x \sim 0.2 - 0.3$ , as compared to that of CT10, whereas down quark distribution becomes larger. This is primarily due to the effect of new  $D\bar{O}$  Run-II WLasy data which probe the ratio of  $d/u$ . Figure 12 shows the comparison in the ratio of  $d/u$  for CT10 and CT10W.

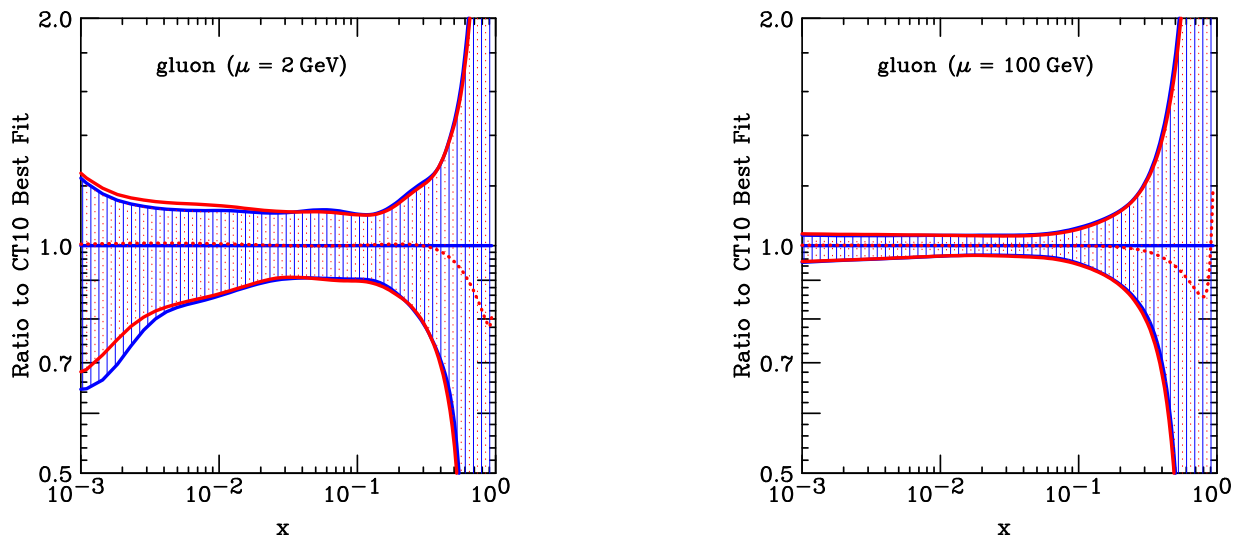


Figure 9: Best fit and uncertainty range for CT10 (solid) and CT10W (dotted) relative to CT10 best fit.

## 7. QUALITY OF FITS TO THE INDIVIDUAL DATA SETS

We will now address the consistency of the CT10(W) global fits with each of the 29 data sets included in the fit. This issue can be explored with several techniques employed by us recently [6–8]. The Fisher’s difference function  $S_n$  (in short,  $S$ ), as shown in Eq. 2, turns out to be convenient for studying the compatibility of the experiments, since its distribution is symmetric and becomes very close to the standard normal distribution even for small values of  $N$  [33]. The theoretical distribution for  $\chi^2$  for  $N \rightarrow \infty$  is approximately Gaussian with the mean and standard deviation of  $N \pm \sqrt{2N}$ , which implies that the distribution for  $S$  approaches a Gaussian one with the mean 0 and standard deviation 1. The utility of  $S$  comes from the fact that its Gaussian approximation is already quite accurate for  $N$  as small as 10, and it becomes symmetric (not skewed in either direction) faster than the

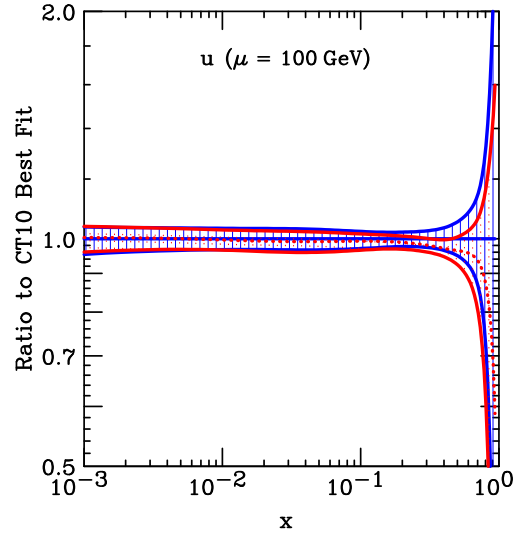
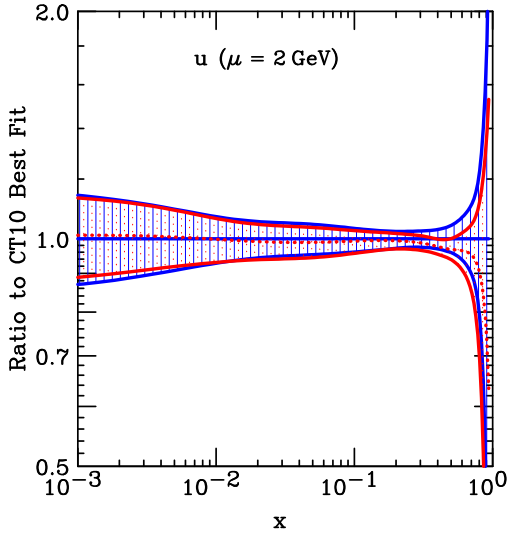


Figure 10: Best fit and uncertainty range for CT10 (solid) and CT10W (dotted) relative to CT10 best fit.

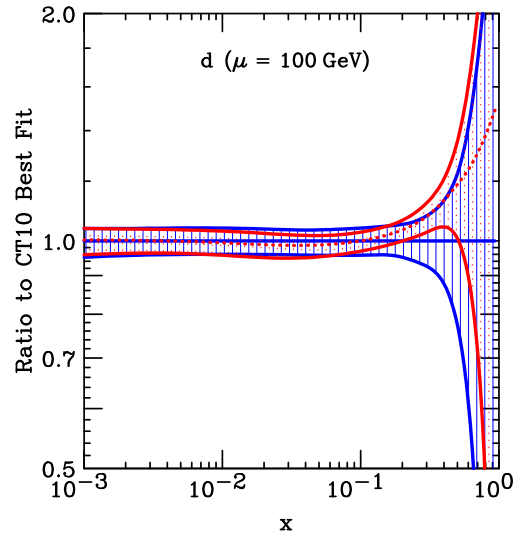
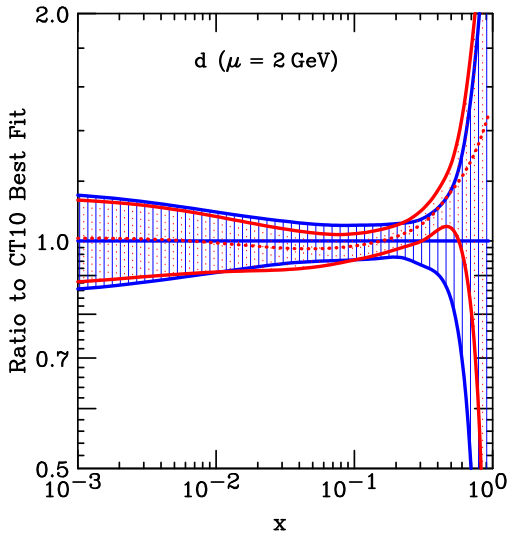


Figure 11: Best fit and uncertainty range for CT10 (solid) and CT10W (dotted) relative to CT10 best fit.

$\chi^2$  distribution itself. The  $S$  values can be used to compare the fit quality among different experiments with different numbers of data points, in a simple manner that avoids lengthier calculations based on the direct analysis of  $\chi^2$ .

The accuracy of the approximation is illustrated by Fig. 13. Here we plot contours of the constant cumulative probability in the plane of  $N$  and  $S$ . The lines correspond to  $S$  values for the cumulative probability ranging from 1% to 99%, for each given  $N$ . Note that the three solid curves, which contain the middle 68% of the distribution, lie very close to  $S = -1, 0,$  and  $+1$ . This is entirely expected to happen for the Gaussian limit  $N \rightarrow \infty$ ; but it is seen here to be a good approximation even down to  $N \approx 10$ . For our purposes, the important curves in Fig. 13 are the top three, which contain cumulative probabilities of

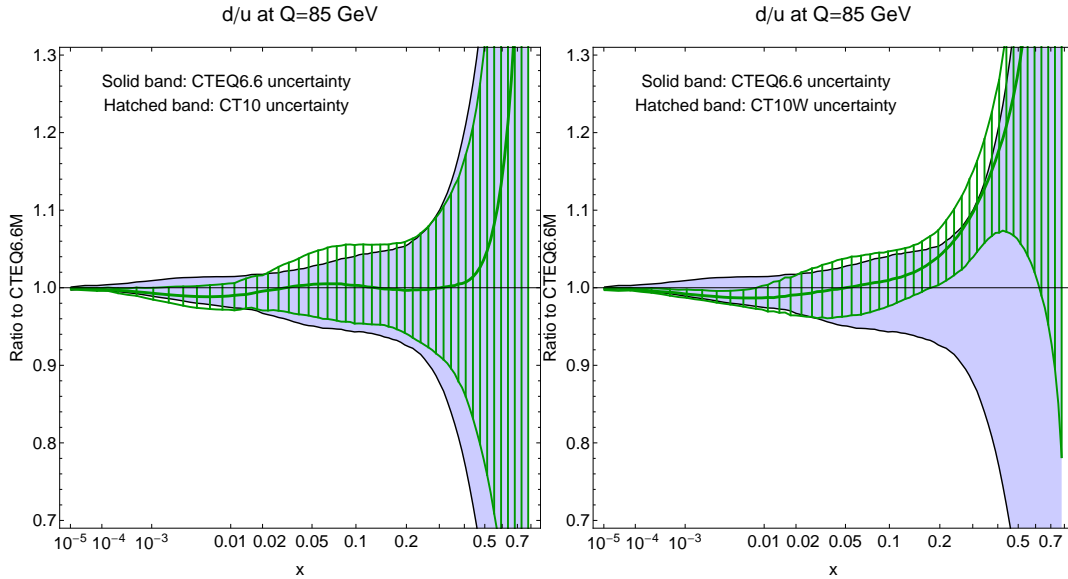


Figure 12: Ratio of  $d/u$  for CT10 (left) and CT10W (right) versus CTEQ6.6 PDFs at  $Q = 85$  GeV.

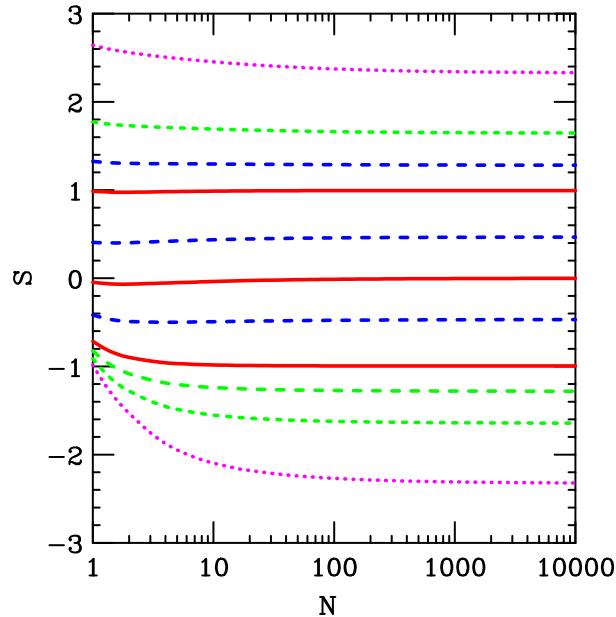


Figure 13: Values of  $S$  corresponding to cumulative probability  $p = 1$  (bottom), 5, 10, 16, 32, 50, 68, 84, 90, 95, and 99% (top). The three solid curves contain the middle 68% of the distribution.

90, 95, and 99%—e.g., the chance of exceeding the value  $S = 1.3$ , 1.6 and 2.4, are 10%, 5%, 1%, respectively, for the range of  $N$  that appears in PDF fitting.

The left side of Fig. 14 shows a histogram of the  $S$ -values for the 29 data sets included in the CT10 best fit. The smooth bell curve is a Gaussian distribution with mean 0 and variance 1. The observed histogram is compatible with a zero mean, but its variance is larger than unity; it would agree better with a Gaussian with the standard deviation of 2 or 3. This indicates some tension between the experiments, of the magnitude compatible

with the findings in other recent studies [6, 8]. It has been observed, for example, that discrepancies between contributions to  $\chi^2$  from individual experiments, which are expected to obey the standard normal distribution, in fact follow a wider normal distribution, with a variance of about 2 [6]. It is also interesting to note that such level of discrepancy appears to be independent of the flexibility of the PDF parametrizations. The right-hand side of Fig. 14 shows a histogram of the  $S$  parameter in a fit with a much more flexible Chebyshev parametrization, which triples the number of the total parameters compared to the CT10 parametrization. In this fit, the  $S$  distribution still preserves the overall, too wide, shape and does not eliminate the two most-outlying points (for the NMC proton data on the right and CCFR  $F_3$  data on the left). The analysis of the  $S$  distribution leads us to believe that non-negligible tensions do exist between the subsets of the current global hadronic data, regardless of the number of free parameters in the PDFs, and contrary to the existing claims of the opposite [34].<sup>2</sup>

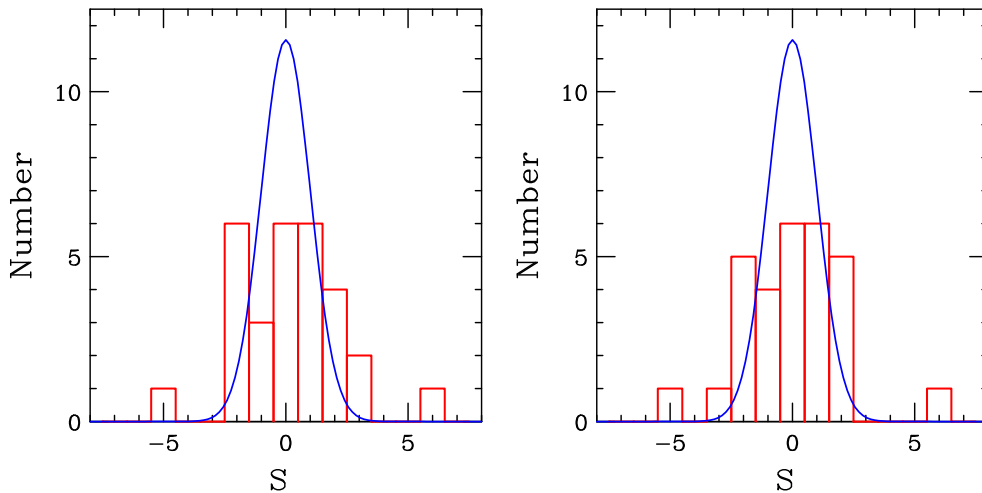


Figure 14: Distribution of the  $S$  parameter across the 29 data sets used in CT10. The left-hand side is the CT10 fit; the right-hand side uses a more flexible parametrization with 71 free parameters.

## 8. APPLICATIONS TO TEVATRON AND LHC PHYSICS

In this section, we examine the impact of the new parton distribution functions on production of  $W$ ,  $Z$ , top quark, Higgs boson and representative new physics signals at the Tevatron Run-II and the LHC (with 7 TeV and 14 TeV). We refer the readers to the published CTEQ6.6 paper [10] for the rationale of selecting these processes to explore the impact of the PDFs on hadron collider phenomenology. In addition, we also comment on a recently published measurement of  $D\bar{O}$  Run-II dijet invariant mass distribution. All through this

<sup>2</sup> By this measure, similar tensions between the experiments appear to exist in the NNPDF2.0 analysis [34]. The overall  $\chi^2=1.27$  of that analysis is larger than our 1.1. The  $S$  parameter distribution of the NNPDF2.0 fit, computed from the breakdown of the  $\chi^2$  values over experiments in Tables 1 and 10 of Ref. [34], is significantly broader than the expected normal distribution, according to a pattern that is roughly analogous to ours.

section, we shall mainly present results predicted with the new PDF sets and compare them to those predicted with CTEQ6.6 PDF sets.

### 8.1. $W$ and $Z$ Physics

Figs. 15 and 16 show CT10 predictions for the charged lepton asymmetry in  $W$  boson production with various transverse momentum ( $p_T^l$ ) cuts on the decay charged lepton and missing transverse energy ( $\cancel{E}_T$ ). Fig. 15 shows the comparison to the Tevatron Run-II  $D\bar{O}$   $W$  electron asymmetry data [21], and Fig. 16 to the Tevatron Run-II  $D\bar{O}$   $W$  muon asymmetry data [22]. For comparison, the CTEQ6.6 predictions are also shown; predictions of those are similar to the CT10 predictions both for the central values and PDF-induced uncertainty bands, except in the large rapidity region ( $|y| > 2$ ) with  $p_T^l > 35$  GeV, where CT10 predicts a somewhat smaller PDF uncertainty. As shown in the figure, the CT10 prediction shows no improvement as compared to the data. (Note that the  $D\bar{O}$  Run-II  $W$  Lasy data are not included in the global fit of CT10 PDF set.)

Figs. 17 and 18 are similar to Figs. 15 and 16, but for CT10W PDFs. In this case, the Tevatron Run-II  $D\bar{O}$   $W$  electron asymmetry data [21], as shown in Figs. 17, and the  $D\bar{O}$   $W$  muon asymmetry data with  $p_T^l > 20$  GeV and  $\cancel{E}_T > 20$  GeV [22], as shown in the first panel of Figs. 18, are included in the global fit (with weights specified in Sec.6) to obtain the CT10W PDF sets. As expected, the CT10W prediction agrees better with Tevatron Run-II data than the CTEQ6.6 prediction. Most noticeably, the PDF-induced uncertainty band from CT10W is much smaller than that from CTEQ6.6 (or CT10). This is because the  $W$  lepton asymmetry data are sensitive to the ratio of  $d/u$ , and the inclusion of these data in the global fit largely reduces the uncertainty in the  $d/u$  ratio. Another noticeable feature in Fig. 18 is that the CT10W prediction cannot describe well the Run-II  $D\bar{O}$   $W$  muon asymmetry data with  $20 \text{ GeV} < p_T^l < 35 \text{ GeV}$  nor  $p_T^l > 35 \text{ GeV}$ .<sup>1</sup> This indicates that the  $D\bar{O}$  Run-II  $W$  muon asymmetry data do not agree well with the counterpart electron asymmetry data. The theory predictions made in the above comparison were obtained using the ResBos calculations [35] which includes the exact  $\alpha_s^2$  correction for  $W$  bosons produced with non-zero transverse momentum. We have checked that this next-to-next-to-leading order (NNLO) effect is small and does not produce sizable change in the shape of the lepton asymmetry distribution as compared to the NNLL-NLO ResBos predictions.

Fig. 19 shows ratios of the experimental data on NLO rapidity distributions of  $Z$  boson (when available), and theoretical predictions for the CT10 and CT10W families of PDFs, to the theoretical prediction based on the CTEQ6.6 best fit, at Tevatron Run-II and LHC. Both CT10 and CT10W give similar predictions as CTEQ6.6, but slightly larger PDF uncertainties than CTEQ6.6 due to the use of more flexible parametrization of non-perturbative PDFs at low energy scale. Furthermore, the CDF Run-II  $Z$  rapidity data appears to favor CT10W over CT10 PDFs, i.e. support the trend suggested by the  $D\bar{O}$  Run-II electron asymmetry data.

Fig. 20 is similar to Fig. 19, but for the rapidity distribution of  $W$  boson at the LHC.

---

<sup>1</sup> These two sets are not included in the CT10 and CT10W fits, because they are incompatible to all other data in our study.

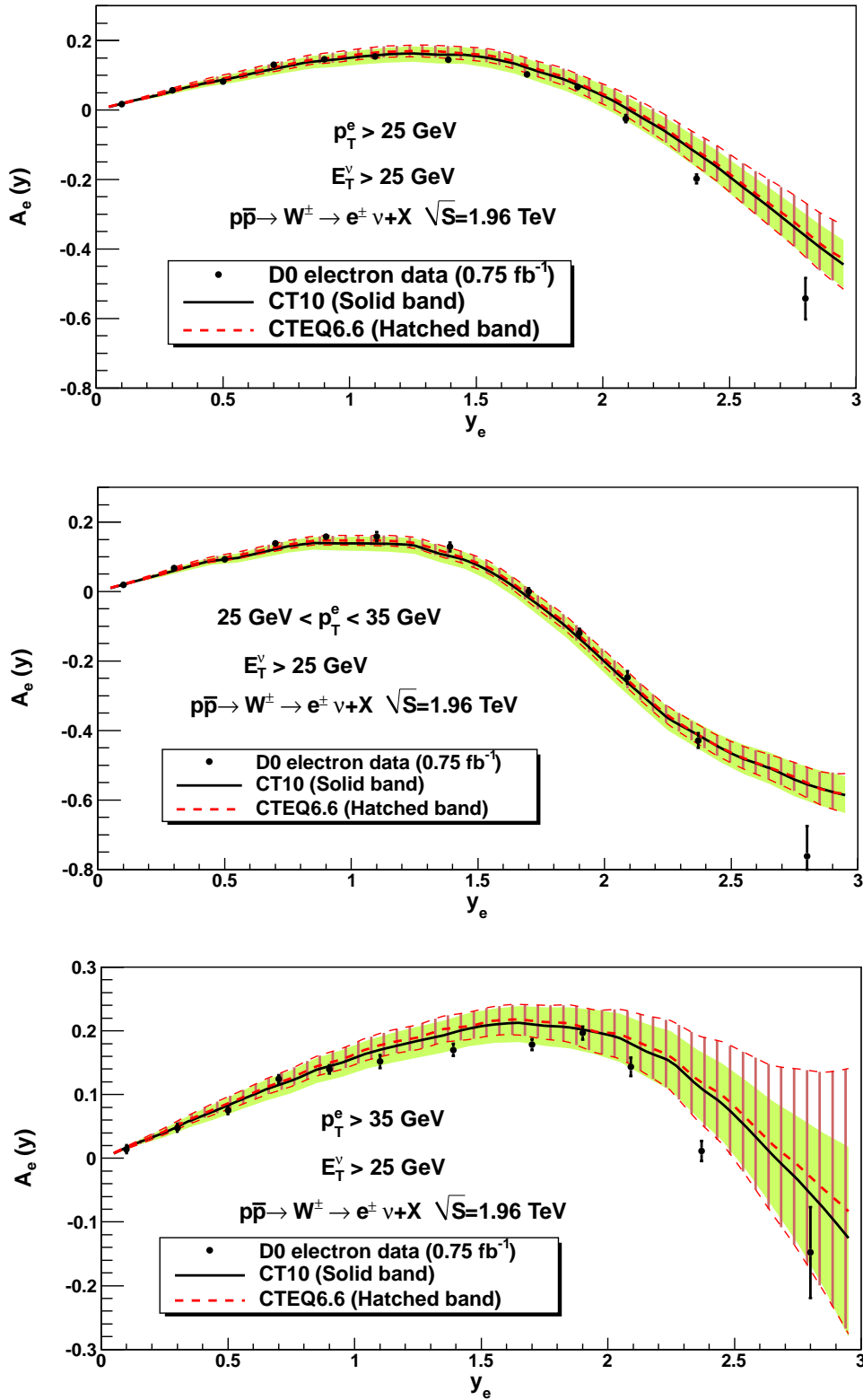


Figure 15: Comparison of the CT10 and CTEQ6.6 predictions to the Tevatron Run-II  $D\bar{O}$  data on the  $W$  electron asymmetry for integrated luminosity of  $0.75 \text{ fb}^{-1}$  [21].

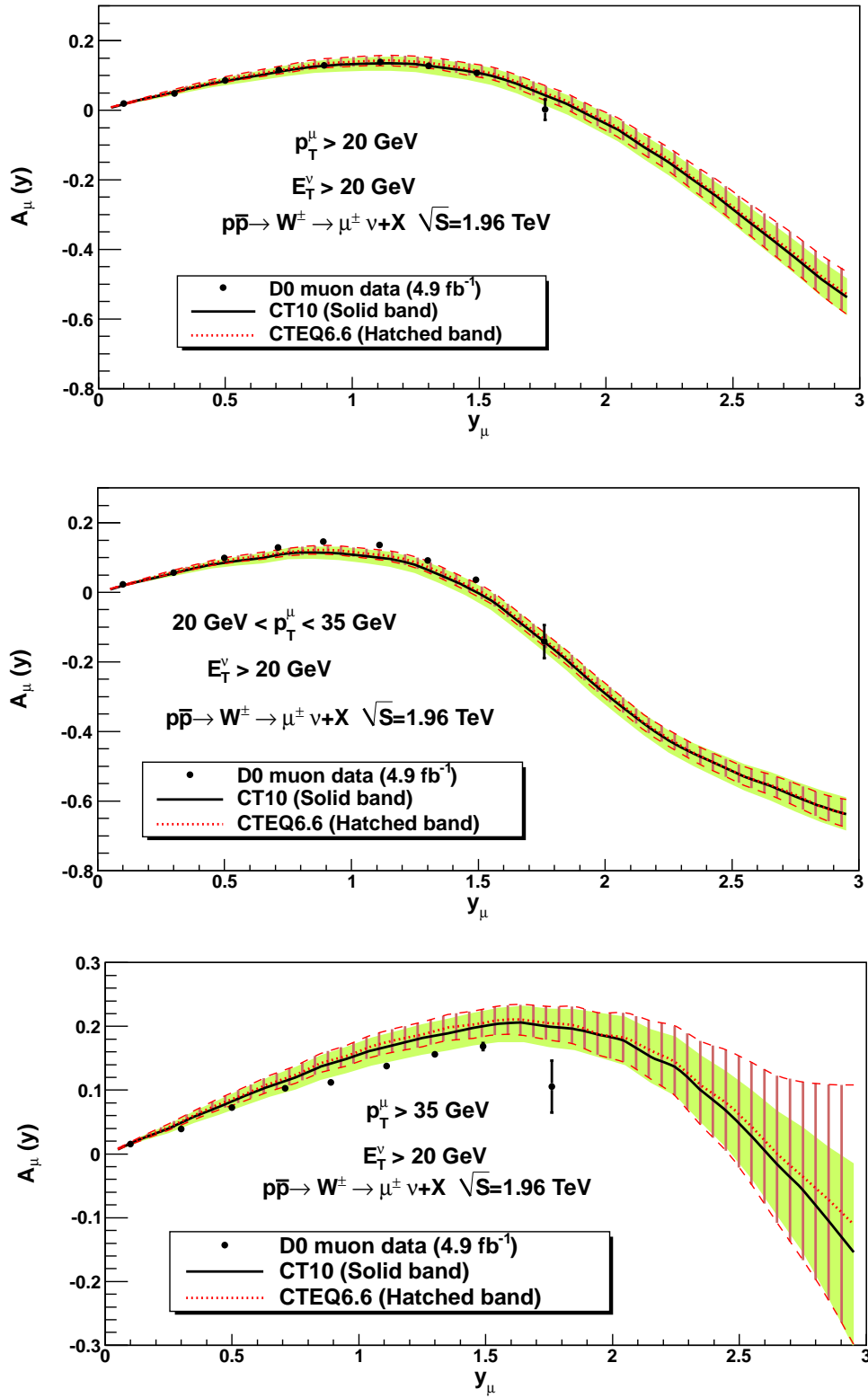


Figure 16: Same as Fig. 15, but for the Tevatron Run-II D0 data on the  $W$  muon asymmetry for integrated luminosity of  $4.9 \text{ fb}^{-1}$  [22].

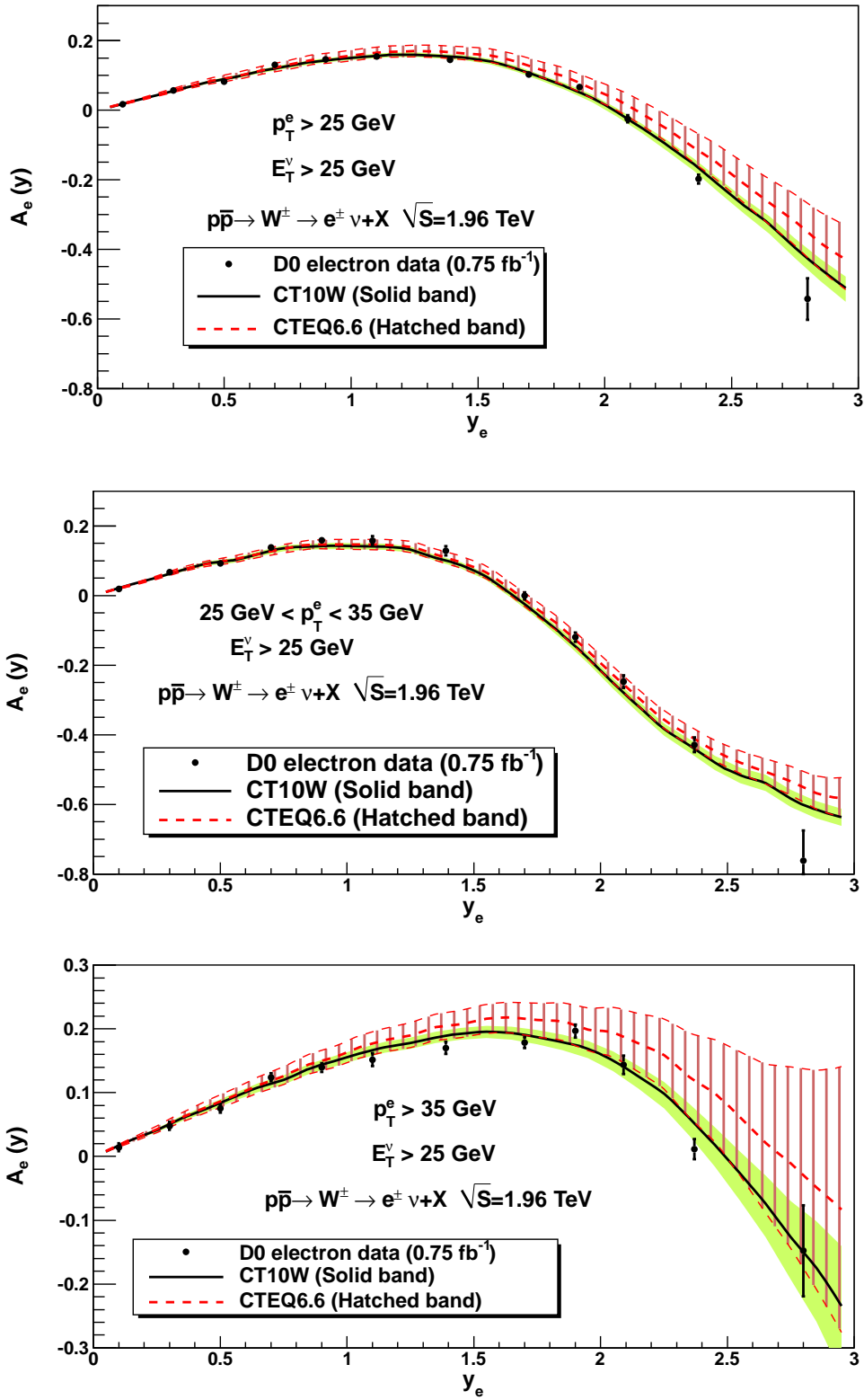


Figure 17: Comparison of the CT10W and CTEQ6.6 predictions to the Tevatron Run-II DØ data on the  $W$  electron asymmetry for integrated luminosity of  $0.75 \text{ fb}^{-1}$  [21].

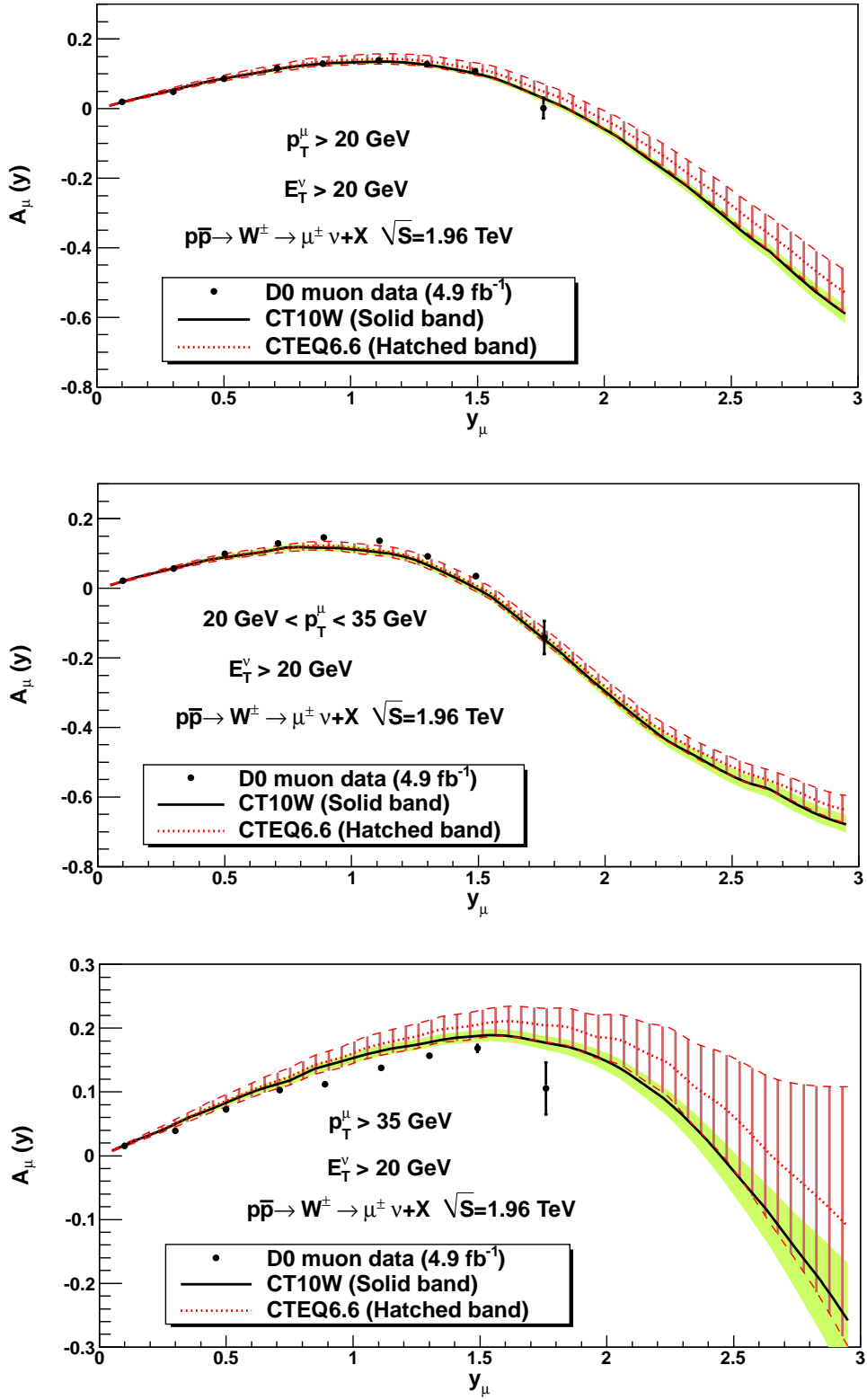


Figure 18: Same as Fig. 17, but for the Tevatron Run-II D0 data on the  $W$  muon asymmetry for integrated luminosity of  $4.9 \text{ fb}^{-1}$  [22].

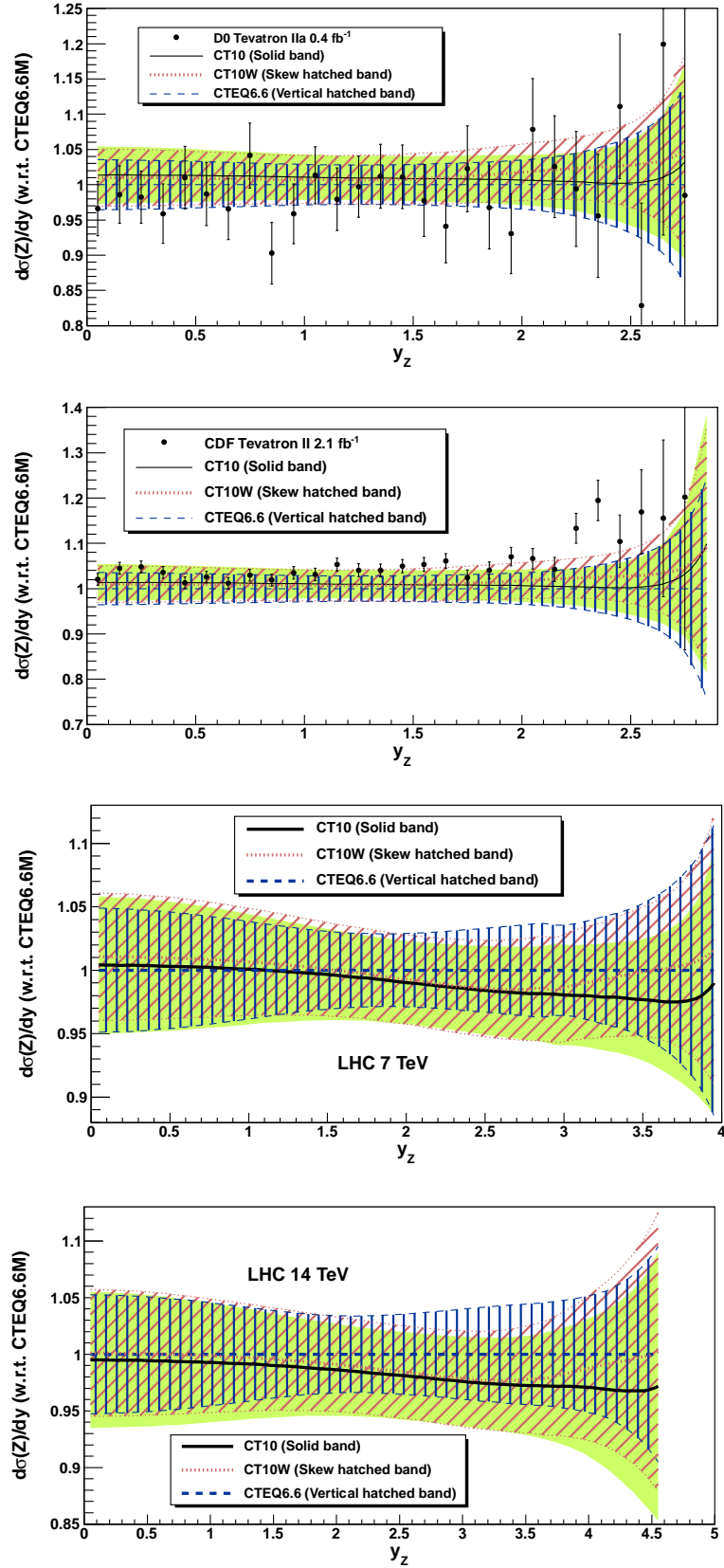


Figure 19: Ratios of the NLO rapidity distributions of Z boson, relative to the CTEQ6.6 best fit, at Tevatron Run-II and LHC.

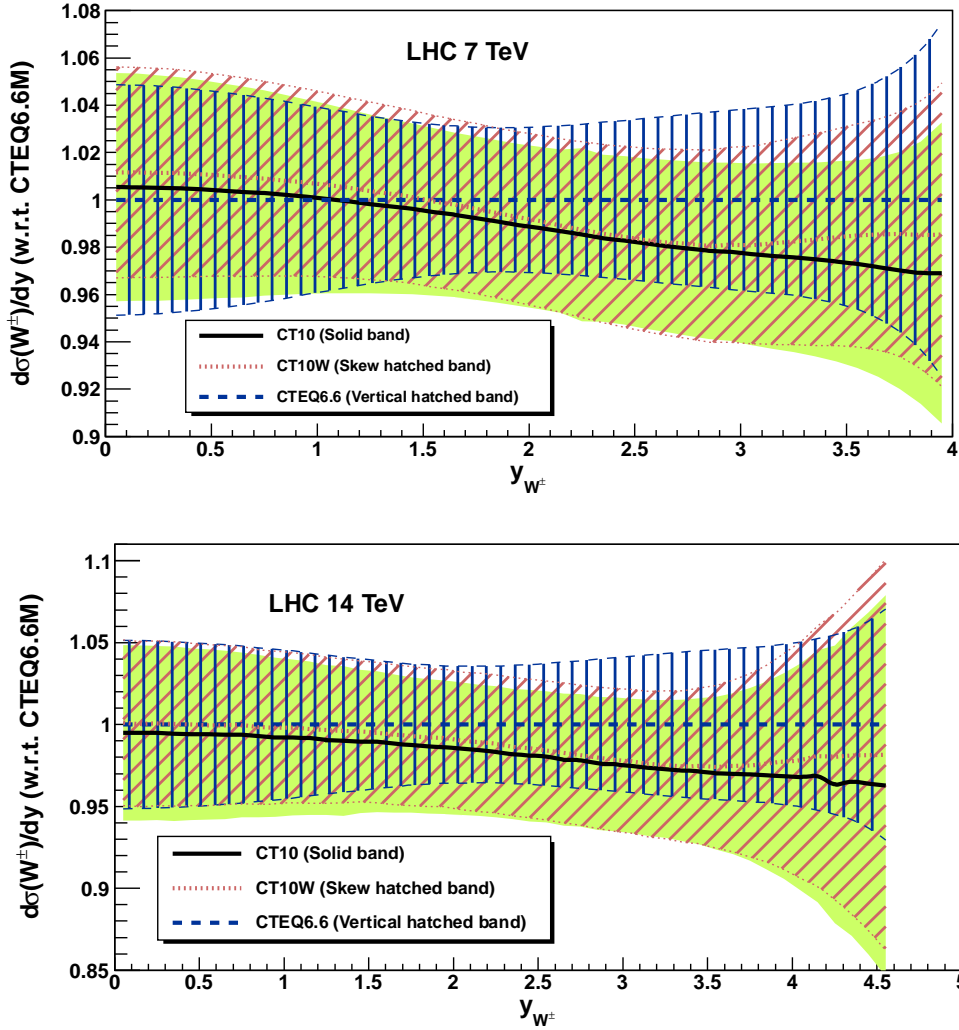


Figure 20: Ratios of the NLO rapidity distributions of  $W$  bosons (including both  $W^+$  and  $W^-$ ), relative to the CTEQ6.6M best fit, at the LHC.

Again, CT10 and CT10W central predictions are similar to those of CTEQ6.6, but have slightly larger PDF uncertainties.

Fig. 21 shows the ratios of rapidity distributions of  $W^+W^-$  to  $Z$ , and  $W^+$  to  $W^-$ , using CTEQ6.6 (blue), CT10 (green) and CT10W (red) PDFs divided by the prediction using CTEQ6.6M, for comparison. For the ratio of the rapidity distribution of  $W^+W^-$  to  $Z$ , both CT10 and CT10W predict wider PDF uncertainties than CTEQ6.6 when the rapidity ( $y$ ) of the boson is less than about 3 at the LHC energies. This is due to more flexible parametrization of the strange (anti-) quark PDF used in the CT10 and CT10W PDFs at low energy scale. However, for the ratio of  $W^+$  to  $W^-$ , CT10 provides slightly smaller PDF uncertainty than CTEQ6.6, and CT10W gives even smaller uncertainty, because the inclusion of the  $D\bar{O}$  Run-II  $W$  lepton asymmetry data improves the constraint on the ratio of down-quark to up-quark PDFs, especially in the large  $x$  region.

Finally, we examine the correlations between the total cross sections of the  $W$  boson and

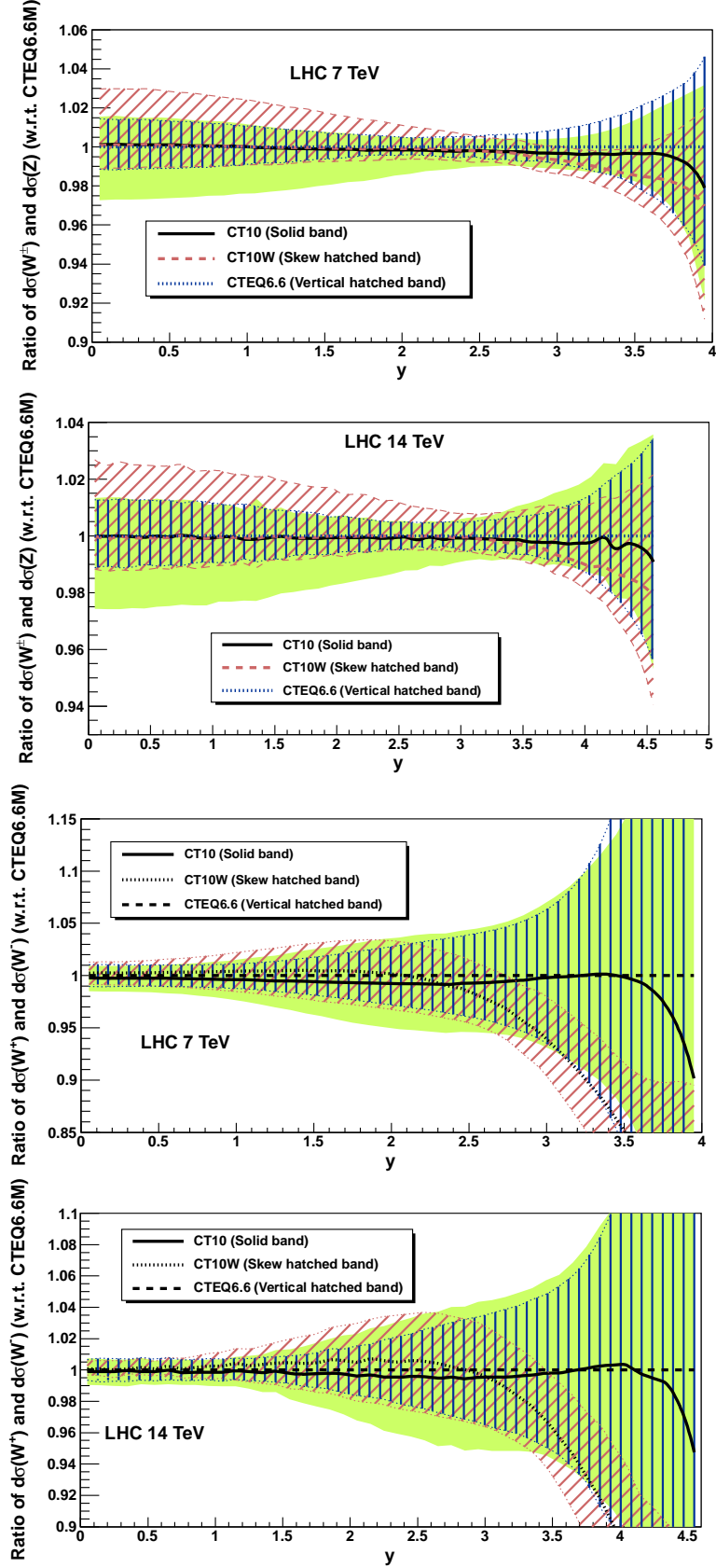


Figure 21: Ratios of rapidity distribution of  $W^+ + W^-$  to  $Z$ , and  $W^+$  to  $W^-$ , using CTEQ6.6 (blue), CT10 (green) and CT10W (red) PDFs divided by the prediction using CTEQ6.6M, for comparison.

$Z$  boson produced at the Tevatron Run-II and the LHC. Following the method described in Ref. [10], we show below the “tolerance ellipse” for various cross sections of  $W^+$ ,  $W^-$  and  $Z$  bosons, calculated at the NLO in QCD, unless specified otherwise.

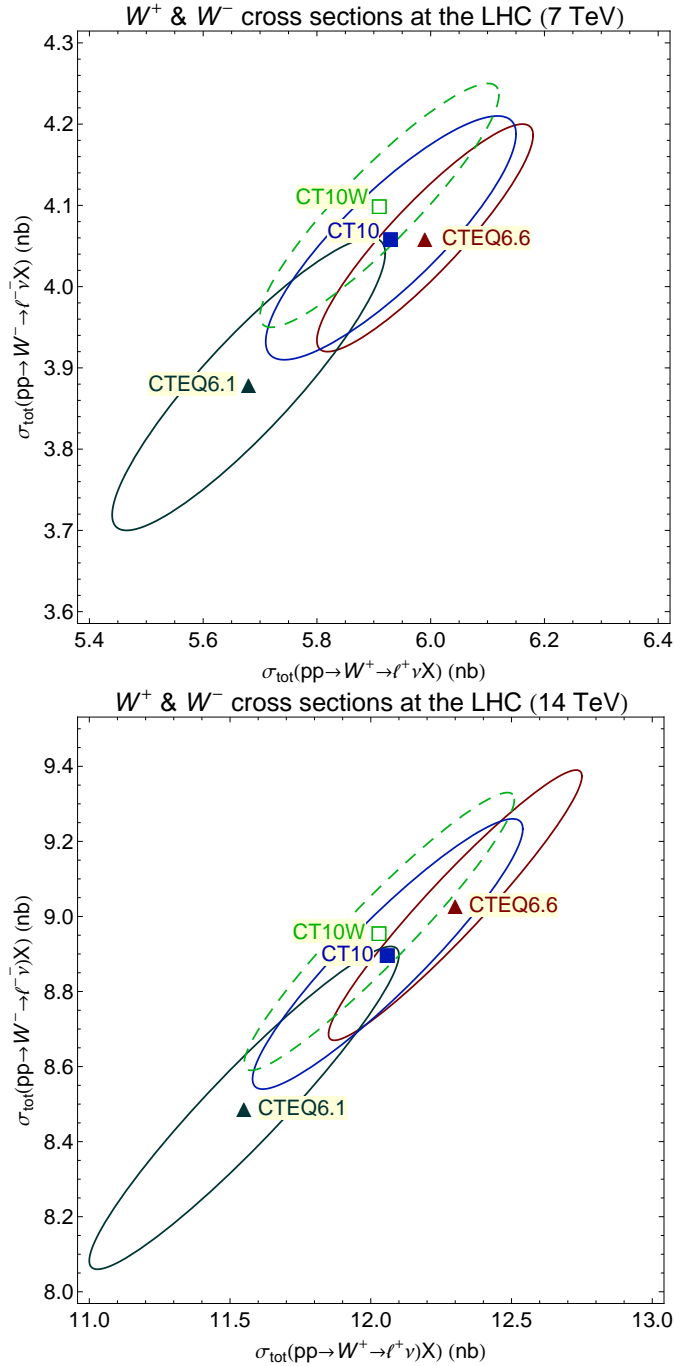


Figure 22:  $W^+$  and  $W^-$  cross sections at the LHC.

Fig. 22 shows the comparison between  $W^+$  and  $W^-$  total cross section at the LHC. CT10 and CT10W provide different predictions for the ratios of  $W^+$  and  $W^-$ , which is mainly due to the change of  $d/u$  ratio.

Fig. 23 shows the comparison between  $W^\pm$  and  $Z$  total cross section at Tevatron Run-II

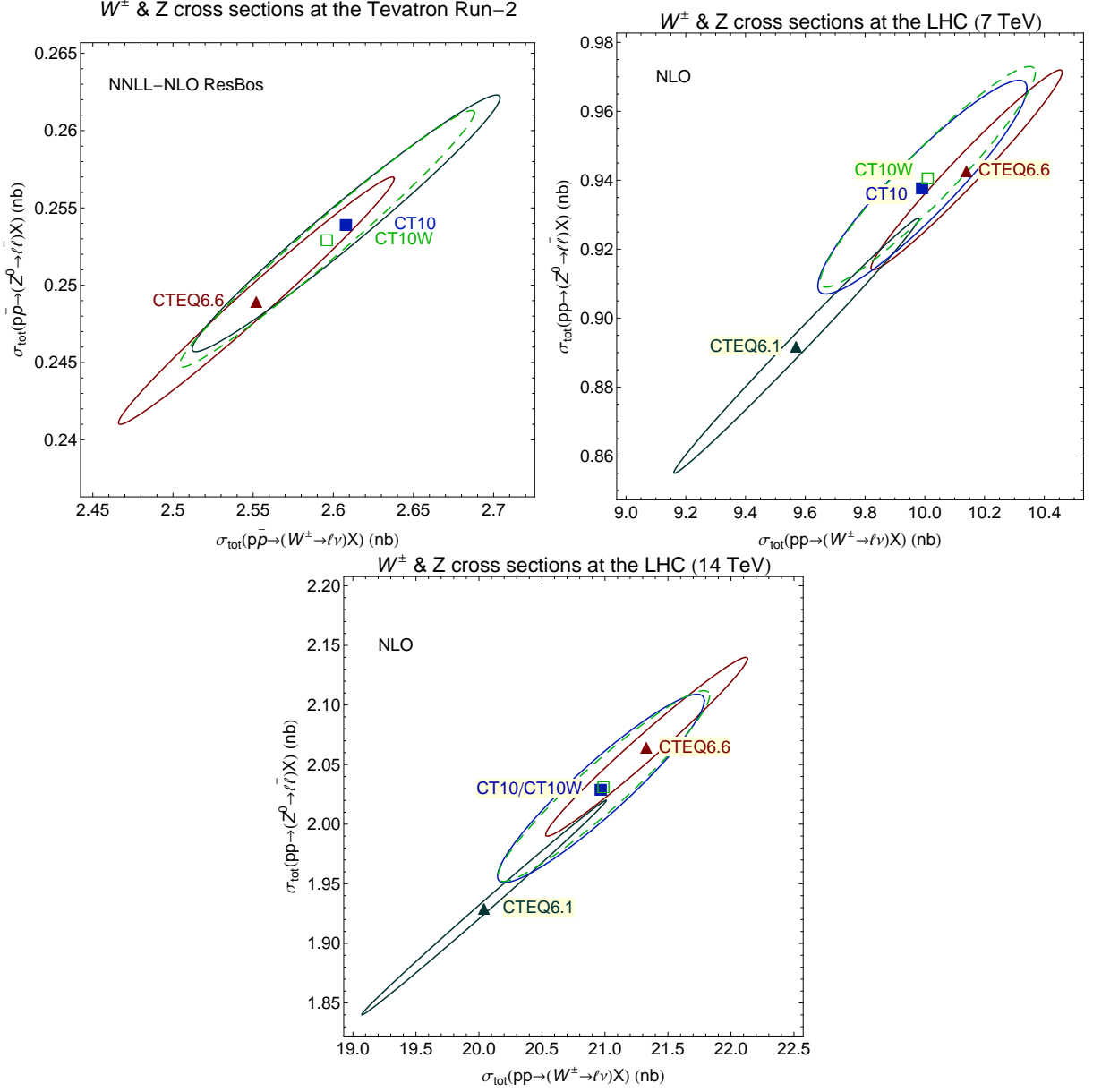


Figure 23:  $W^\pm$  and  $Z$  cross sections at Tevatron Run-II and LHC.

and the LHC. At the Tevatron, CT10 and CT10W provide different predictions for both the total cross sections of  $W^\pm$  and  $Z$ , but the ratio of  $W^\pm$  and  $Z$  are the same as CTEQ6.6. However, at the LHC CT10 and CT10W shows different ratios of  $W^\pm$  and  $Z$  total cross sections, which is mainly due to the change of strange quark PDF.

## 8.2. Other Significant Processes

To further examine the impact of the new PDFs on hadron collider phenomenology, we compare total cross sections of some selected production processes at the Tevatron Run-II and the LHC (with 7 TeV, 10 TeV and 14 TeV). The list of production processes includes the

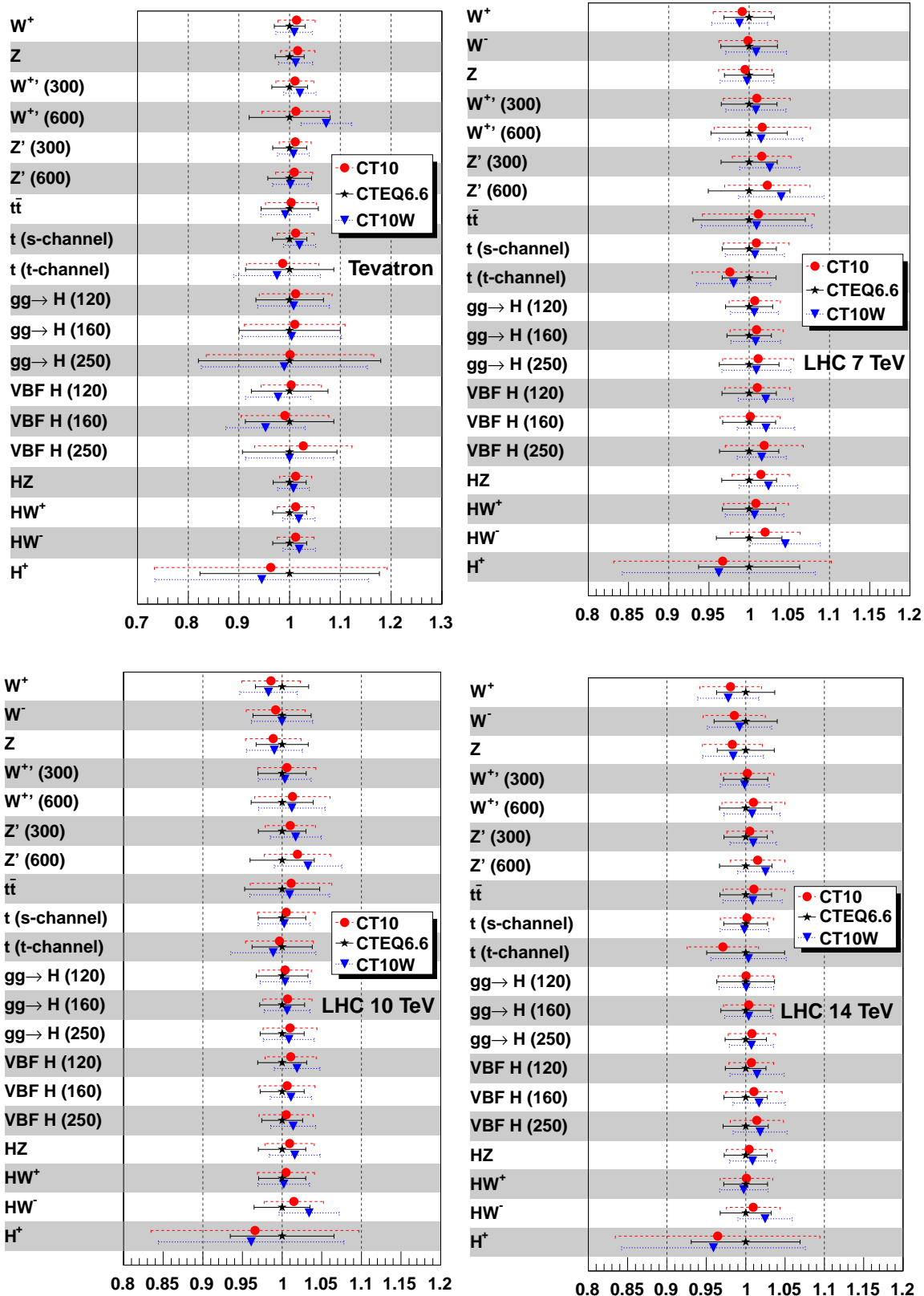


Figure 24: Ratios of NLO total cross sections using CT10 and CT10W to those using CTEQ6.6M PDFs.

production of  $W^+$ ,  $W^-$ ,  $Z$ , top-quark pair ( $t\bar{t}$ ), s-channel single-top, t-channel single-top, Higgs boson via gluon fusion ( $gg \rightarrow H$ , with Higgs boson mass being 120 GeV, 160 GeV or 250 GeV) [36], Higgs boson via weak gauge boson fusion ( $VV \rightarrow H$ ) [37], the associated production of Higgs boson and weak gauge boson ( $HW^+$ ,  $HW^-$  and  $HZ$ ), the “sequential” heavy weak bosons ( $W'^+$  and  $Z'$ , with mass being 300 GeV or 600 GeV), and a 200 GeV charged Higgs boson via  $c\bar{s} \rightarrow H^+$  as predicted in the two-Higgs-doublet model. (The couplings of  $W'^+$  and  $Z'$  to fermions are taken to be the same as those in the Standard Model.)

Fig. 24 shows the ratios of various NLO total cross sections using CT10 and CT10W to those using CTEQ6.6 PDFs. For most of the cross sections, CT10 and CT10W give similar predictions and uncertainties. It is evident that the central values of CT10 and CT10W predictions are in good agreement with CTEQ6.6 (well within the PDF-induced uncertainty band), while the uncertainty bands of CT10 and CT10W are generally larger than those of CTEQ6.6 at the LHC energies, and about the same at Tevatron Run-II energy. This can be attributed to the new theoretical treatment discussed in Sec. 2. However, at Tevatron Run-II, both CT10 and CT10W give somewhat smaller uncertainty for top quark pair production mainly due to the better determination of up- and down-quark PDFs at the relevant  $x$  values. Furthermore,  $W'^+$  (600 GeV) production with CT10W PDFs is enhanced at the Tevatron Run-II energy due to a sizable increase in the down quark distribution at high  $x$  values, which is driven by the DØ Run-II  $W$  lepton asymmetry data. On the contrary, the  $Z'$  (600 GeV) production rate is about the same as CTEQ6.6 prediction at the Tevatron energy, because the variation in cross sections of the  $u\bar{u}$  and  $d\bar{d}$  subprocesses more or less cancel. (The coupling of  $Z$  boson to down-quark is stronger than to up-quark, and in large  $x$  region CT10W  $d$ -PDF increases while  $u$ -PDF decreases, as compared to CTEQ6.6.)

At the LHC energies, total cross sections of some production processes change as compared to the CTEQ6.6 predictions. For example, at 14 TeV LHC, the total cross sections of  $W$  and  $Z$  bosons decrease while those of  $Z'$  and  $HW^-$  increase. The decrease in the central value of the  $c\bar{s} \rightarrow H^+$  cross section in CT10 and CT10W predictions is due to the decrease in the strange quark PDF at the relevant  $x$  values; however, with a much larger PDF uncertainty present in CT10 and CT10W than in CTEQ6.6.

### 8.3. Dijet Invariant Mass Distributions

Recently, DØ Collaboration reported their measurement of the dijet invariant mass distribution [38] in which comparison was made to a theory calculation (with FastNLO code [39]) using the CTEQ6.6M PDF set with both normalization and factorization scales set to be the average of the transverse momentum ( $p_T$ ) of the two jets,  $\langle p_T \rangle = (p_T^{jet-1} + p_T^{jet-2})/2$ . In Fig. 2 of [38], it appears that the CTEQ6.6M PDF cannot describe their data in the large di-jet invariant mass region. Below, we shall re-examine the above analysis with the choice of the hard scale that is in accord with the analysis of the Tevatron Run-II inclusive jet data (included in both CTEQ6.6 and CT10 fits). Namely, we shall take both normalization and factorization scales to be  $\langle p_T \rangle / 2$  to compare with the DØ Run-II di-jet invariant mass distribution. The reason for this choice of the scale is that the same experimental events used in the inclusive jet measurement are used for the di-jet invariant mass measurement by the DØ Collaboration.

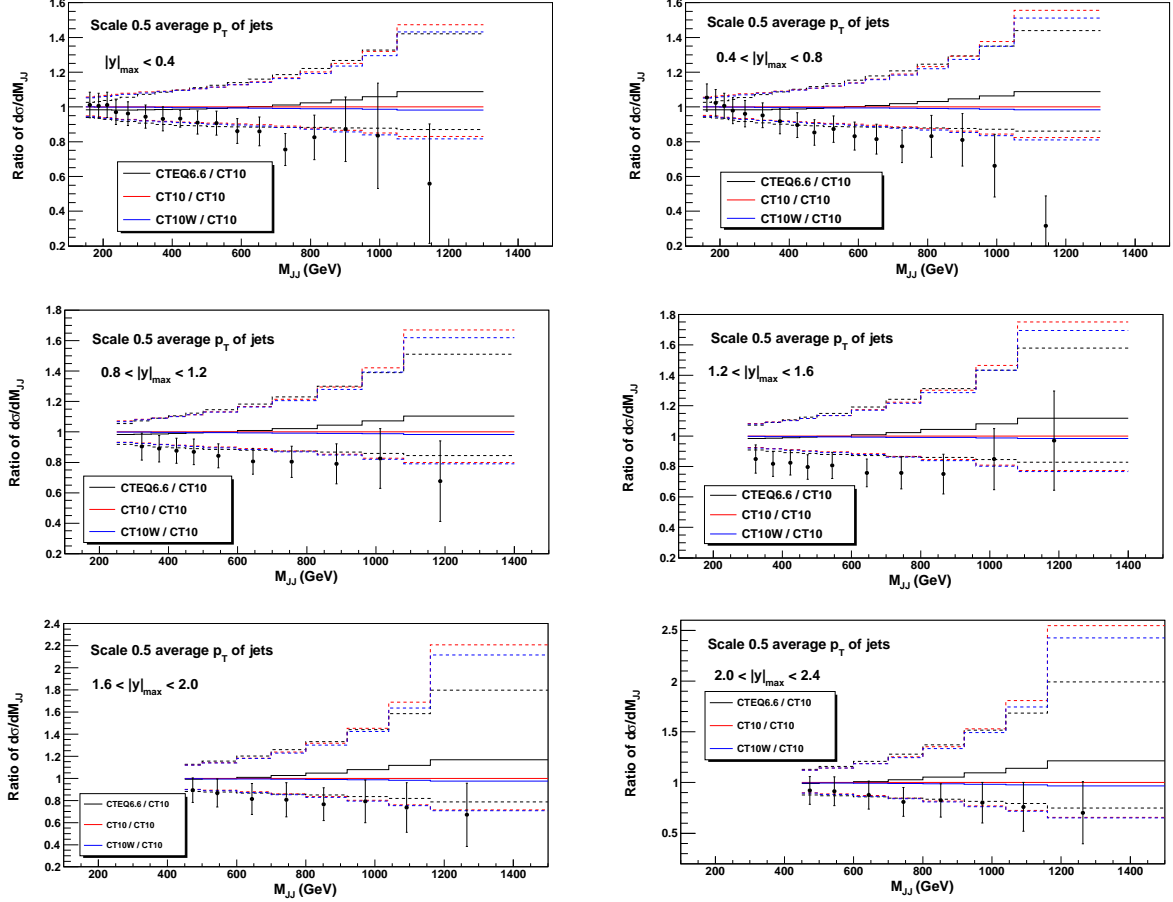


Figure 25: Ratios of NLO dijet invariant mass distribution at Tevatron Run II, using CTEQ6.6 (black), CT10 (red) and CT10W (blue) PDFs over CT10 best fit (CT10.00) PDFs.

Fig. 25 shows the ratios of NLO di-jet invariant mass distribution  $d\sigma/dM_{jj}$  at Tevatron, Run-II using CTEQ6.6 (black), CT10 (red) and CT10W (blue) PDFs divided by the CT10 best fit (CT10.00), with the renormalization and factorization scales chosen to be half of the average transverse momentum of the two leading jets, i.e.  $\langle p_T \rangle / 2$ . The  $D\bar{O}$  data, with statistical and systematic errors added in quadrature, are also shown. We find that with this choice of the scale, all three PDF sets are in better agreement with the data than the conclusions of the  $D\bar{O}$  paper [38] indicate, although an overall systematic shift, of order of systematic shifts observed in the CT09 study of related single-inclusive jet distributions [2], would further improve the agreement. As shown in the figure, the predictions for the central fits of CT10 and CT10W PDFs are close to each other and closer to the data than CTEQ6.6. The extent of CTEQ6.6, CT10, and CT10W PDF uncertainty bands in this ratio is larger by a factor of two than that of MSTW2008NLO eigenvector sets – so that our predictions agree with the MSTW2008NLO predictions, if our estimates of the PDF uncertainty, rather than those of MSTW2008NLO, are used. This observation is consistent with the analysis of di-jet invariant mass distribution of CDF Run-II data [38] which also shows a sizable uncertainty band with CTEQ6.6 PDFs. The lower side of the error bands does not change as much as the upper side, because the production of di-jet events with large invariant mass and rapidity is dominated by quark-quark or quark-antiquark scatterings, followed by

quark-gluon scatterings. Since the quark distributions are relatively better determined at medium to large  $x$  values, the differential cross section of di-jet invariant mass distribution cannot become too small. (The quark-gluon scattering process can only increase the cross sections.)

## 9. CONCLUSIONS

As the LHC is reporting its first cross sections, it becomes even more important to provide the best tools necessary for accurate predictions and comparisons to these cross sections. We have produced two new PDF sets, CT10 and CT10W, intended for comparisons to data at the Tevatron and LHC. The two PDF sets include new data, primarily, the DIS combined data sets from HERA [3], the rapidity distribution of  $Z^0$  production at the Tevatron, and the Tevatron Run-II  $W$  lepton asymmetry data from the DØ Collaboration, as well as several improvements to the global fitting procedure. The latter includes more flexible PDF parameterizations, the treatment of experimental normalizations in the same manner as other systematic uncertainties, the removal of weights associated with the data sets (except for the  $W$  lepton asymmetry data in the case of CT10W), and a more dynamical determination of the allowed tolerance along each eigenvector direction.

Due to the difficulty in fitting both the Tevatron Run-II  $W$  lepton asymmetry data and the other data sets in the global analysis (primarily, the data from the NMC experiment), we have produced two new families of PDFs, CT10 and CT10W. CT10 is obtained without using the new DØ Run-II  $W$  lepton asymmetry data, while CT10W contains those high luminosity data with added weights to ensure reasonable agreement. The resulting predictions for LHC benchmark cross sections, at both 7 TeV and 14 TeV, are generally consistent with those from the older CTEQ6.6 PDFs, in some cases with a slightly larger uncertainty band. The latter is a result of the greater flexibility included in this new generation of global fits. Most noticeable differences in various cross sections, such as the charged Higgs boson and extra heavy gauge boson production, are induced by the strange-quark PDF, the gluon PDF in the small- $x$  region, and the up-quark and down-quark PDFs in the medium to large  $x$  region.

As compared to CTEQ6.6 prediction, both CT10 and CT10W predict a smaller PDF induced uncertainty in the total cross section of the top-quark pair production at the Tevatron Run-II. No great differences are observed for LHC predictions between the CT10 and CT10W PDF sets, except those observables which are sensitive to the ratio of down-quark to up-quark PDFs. One example is the ratio of the rapidity distributions of the  $W^-$  to  $W^+$  predicted at LHC.

There are 26 free parameters in both new PDF sets; thus, there are 26 eigenvector directions and a total of 52 error PDFs for both CT10 and CT10W. The CT10 and CT10W PDF error sets, along with the accompanying  $\alpha_s$  error sets, allow for a complete calculation of the combined PDF+ $\alpha_s$  errors for any observable [40]. These two sets constitute the most comprehensive and up-to-date PDFs for use for predictions at the Tevatron and LHC. All the relevant PDF sets discussed in this paper are available from internet [41].

*Acknowledgements* We thank A. Glazov for useful information on the implementation of HERA-1 correlated errors, and M. Wobisch for DØ Run-II di-jet invariant mass data. We also thank S. Forte, H. Schellman, D. Stump, R. Thorne, J. Zhu, and CTEQ members for useful discussions. CPY and HLL would also like to thank the hospitality of National

$x$ range	CT10.00, comb.		CT10-like, sep.		CTEQ6.6M	
	$N$	$\chi^2/N$	$N$	$\chi^2/N$	$N$	$\chi^2/N$
$<0.001$	63	<b>1.19</b>	68	<b>0.81</b>	68	<b>0.84</b>
$0.001-0.1$	298	0.94	485	0.92	485	0.92
$>0.1$	150	<b>1.43</b>	257	<b>1.26</b>	257	<b>1.25</b>

Table III: Numbers of data points ( $N$ ) and  $\chi^2/N$  found in the CT10 best fit to the combined (CT10.00) and separate (CT10-like) HERA-1 data sets, as well as in the CTEQ6.6M fit.

Center for Theoretical Sciences in Taiwan and (for CPY) Center for High Energy Physics, Peking University, in China, where part of this work was done. This work was supported in part by the U.S. DOE Early Career Research Award DE-SC0003870; by the U.S. National Science Foundation under grant PHY-0855561; by the National Science Council of Taiwan under grants NSC-98-2112-M-133-002-MY3 and NSC-99-2918-I-133-001; by LHC Theory Initiative Travel Fellowship awarded by the U.S. National Science Foundation under grant PHY-0705862; and by Lightner-Sams Foundation.

#### Appendix A: Agreement of QCD theory with the combined HERA-1 data

In this Appendix, we provide additional details on the comparison of CT10 predictions with the combined HERA data, and the origin of some increase in  $\chi^2$  that is observed when independent HERA data sets are combined. The  $\chi^2/N$  values in the intervals  $x < 0.001$ ,  $0.001 < x < 0.1$ , and  $x > 0.1$ , found in the CT10 best fit to the combined (CT10.00) and separate (CT10-like) HERA-1 data sets, as well as in the CTEQ6.6M fit, are listed in Table III. At  $x < 0.001$ ,  $\chi^2/N$  is about 1.19 for the combined HERA-1 set, vs. 0.81-0.84 in the fits to the separate sets. At  $x > 0.1$ , where irregular scatter is obvious in the plots of both  $e^+p$  and  $e^-p$  NC sets (cf. Fig. 1),  $\chi^2/N$  is increased upon the combination of the data sets from 1.25 to 1.43.

To see if these increases in  $\chi^2$  may be caused by systematic discrepancies, we plot histograms of  $\chi^2$  residuals for each data point  $k = 1, \dots, N$ ,

$$\Delta_k = \left( \frac{D_k - T_k(\{a_{\text{best-fit}}\}) - \sum_{\alpha}^{N_{\lambda}} \lambda_{\alpha, \text{best-fit}} \beta_{k\alpha}}{s_k} \right)^2,$$

in each  $x$  range listed in Table III. (See Sec. 4.) In an excellent fit, the residuals follow a standard normal distribution, with a mean of zero and a unit width. A non-zero mean observed in the actual  $\Delta_k$  distribution would indicate a systematic discrepancy affecting the whole histogrammed set of points; on the other hand, a smaller or larger than normal width may be due to unaccounted random effects (see Appendix B.2 in Ref. [17]).

Distributions of the residuals for the best fits to the combined and separate HERA-1 sets are plotted in Fig. 26. At  $0.001 < x < 0.1$  (central figure), frequencies of the residuals agree well with the standard distribution, regardless of whether the HERA-1 sets are separate or combined. At  $x < 0.001$ , the mean of the residual distribution remains consistent with zero upon the combination of the data sets, while the width of the distribution increases. The

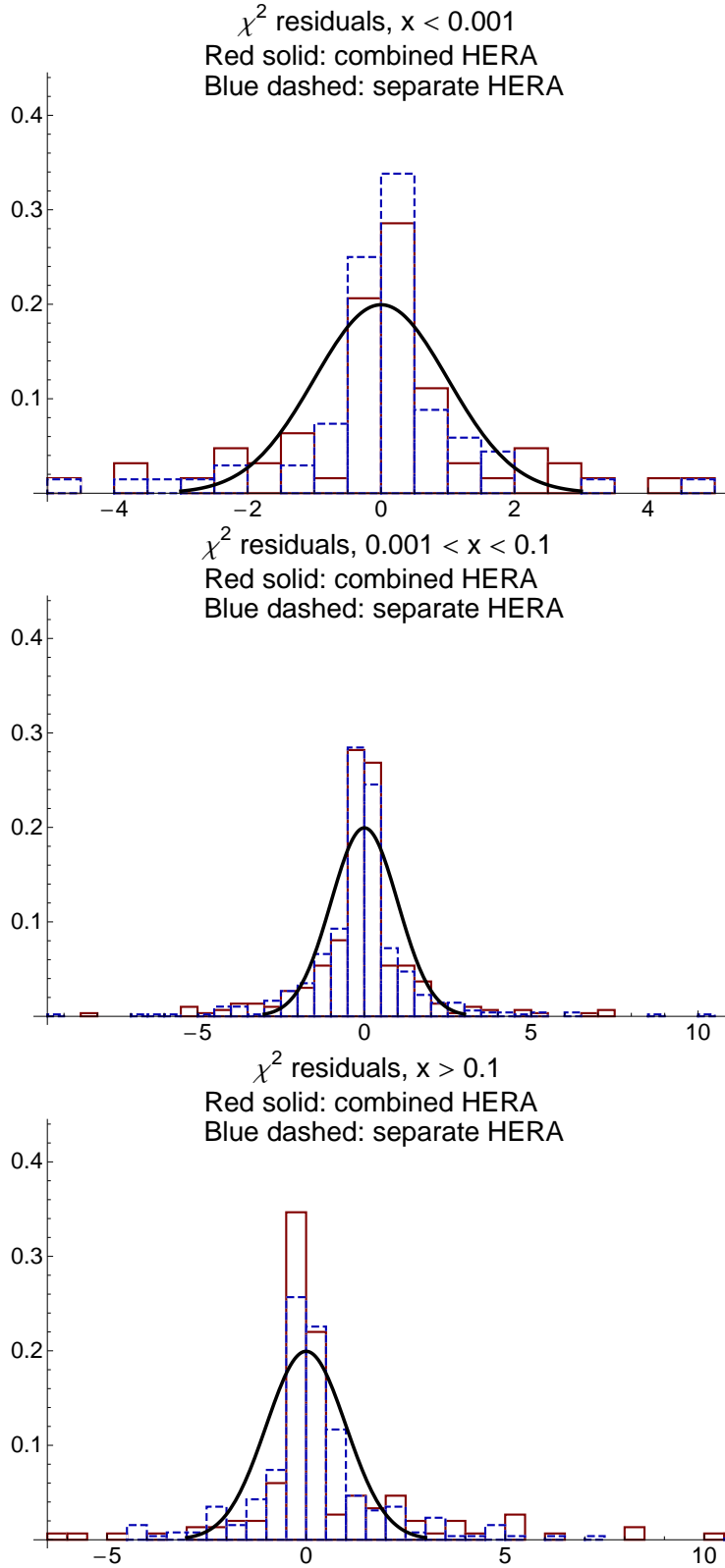


Figure 26: Comparison of frequency distributions of reduced  $\chi^2$  residuals for neutral current HERA data at in the CT10 fits to the combined HERA set (solid lines) and separate HERA data sets (dashed lines), at  $x < 0.001$  (upper figure),  $0.001 < x < 0.1$  (middle figure) and  $x > 0.1$  (lower figure).

residual distribution at  $x > 0.1$  also widens and changes the shape, with more residuals having small negative values or large positive (outlier) values, as compared to the fit to the separate sets. Neither of these patterns indicates systematic deviations of the data from NLO QCD theory.<sup>5</sup> On the other hand, the histograms are suggestive of significant point-to-point random fluctuations in the NC DIS data at  $x < 0.001$  and  $x > 0.1$ , which appear to be exacerbated when the systematic uncertainties are reduced through the combination of the data sets. The origin of these fluctuations requires further investigation.

- 
- [1] A. D. Martin, W. J. Stirling, R. S. Thorne, and G. Watt, *Eur. Phys. J.* **C63**, 189 (2009), arXiv:0901.0002.
  - [2] J. Pumplin *et al.*, *Phys. Rev.* **D80**, 014019 (2009), arXiv:0904.2424.
  - [3] H1, F. D. Aaron *et al.*, *JHEP* **01**, 109 (2010), arXiv:0911.0884.
  - [4] R. D. Ball *et al.*, *Nucl. Phys.* **B838**, 136 (2010), arXiv:1002.4407.
  - [5] S. Alekhin, J. Blumlein, S. Klein, and S. Moch, *Phys. Rev.* **D81**, 014032 (2010), arXiv:0908.2766.
  - [6] J. Pumplin, *Phys. Rev.* **D81**, 074010 (2010), arXiv:0909.0268.
  - [7] J. C. Collins and J. Pumplin, (2001), arXiv:hep-ph/0105207.
  - [8] J. Pumplin, *Phys. Rev.* **D80**, 034002 (2009), arXiv:0904.2425.
  - [9] J. R. Brown, *Journal of the Academy of Marketing Science* **2**, 447 (1974).
  - [10] P. M. Nadolsky *et al.*, *Phys. Rev.* **D78**, 013004 (2008), arXiv:0802.0007.
  - [11] F. James and M. Roos, *Comput. Phys. Commun.* **10**, 343 (1975).
  - [12] V. N. Gribov and L. N. Lipatov, *Yad. Fiz.* **15**, 781 (1972), [*Sov. J. Nucl. Phys.* **15** 438 (1972)].
  - [13] G. Altarelli and G. Parisi, *Nucl. Phys.* **B126**, 298 (1977).
  - [14] Y. L. Dokshitzer, *Sov. Phys. JETP* **46**, 641 (1977).
  - [15] J. Pumplin *et al.*, *Phys. Rev.* **D65**, 014013 (2001), arXiv:hep-ph/0101032.
  - [16] D. Stump *et al.*, *Phys. Rev.* **D65**, 014012 (2001), arXiv:hep-ph/0101051.
  - [17] J. Pumplin *et al.*, *JHEP* **07**, 012 (2002).
  - [18] P. M. Nadolsky *et al.*, *Phys. Rev.* **D78**, 013004 (2008), arXiv:0802.0007.
  - [19] J. Pumplin *et al.*, *Phys. Rev.* **D80**, 014019 (2009), arXiv:0904.2424.
  - [20] CDF, T. Aaltonen *et al.*, *Phys. Rev. Lett.* **102**, 181801 (2009), arXiv:0901.2169.
  - [21] D0, V. M. Abazov *et al.*, *Phys. Rev. Lett.* **101**, 211801 (2008), arXiv:0807.3367.
  - [22] D0, V. M. Abazov *et al.*, *Phys. Rev.* **D77**, 011106 (2008), arXiv:0709.4254.
  - [23] [https://www.desy.de/h1zeus/combined\\_results/](https://www.desy.de/h1zeus/combined_results/).
  - [24] F. Caola, S. Forte, and J. Rojo, *Phys. Lett.* **B686**, 127 (2010), arXiv:0910.3143.
  - [25] P. M. Nadolsky and Z. Sullivan, (2001), hep-ph/0110378.
  - [26] H. L. Lai *et al.*, *Phys. Rev.* **D55**, 1280 (1997), arXiv:hep-ph/9606399.
  - [27] New Muon., M. Arneodo *et al.*, *Phys. Lett.* **B364**, 107 (1995), arXiv:hep-ph/9509406.
  - [28] BCDMS, A. C. Benvenuti *et al.*, *Phys. Lett.* **B223**, 485 (1989).
  - [29] BCDMS, A. C. Benvenuti *et al.*, *Phys. Lett.* **B237**, 592 (1990).
  - [30] CDF, F. Abe *et al.*, *Phys. Rev. Lett.* **74**, 850 (1995), arXiv:hep-ex/9501008.

---

<sup>5</sup> In this light, the CT10 fit does not confirm deviations from the NLO DGLAP evolution at small  $x$  that has been recently reported by the NNPDF group [24].

- [31] A. Accardi *et al.*, Phys. Rev. **D81**, 034016 (2010), arXiv:0911.2254.
- [32] R. S. Thorne, A. D. Martin, W. J. Stirling, and G. Watt, (2010), arXiv:1006.2753.
- [33] R. A. Fisher, *Statistical methods for research workers* (Oliver and Boyd, Edinburgh, 1925), chap. 4, an Internet version of the 1st edition at <http://psychclassics.yorku.ca/Fisher/Methods/>.
- [34] R. D. Ball *et al.*, Nucl. Phys. **B838**, 136 (2010), arXiv:1002.4407.
- [35] C. Balazs, J.-w. Qiu, and C. P. Yuan, Phys. Lett. **B355**, 548 (1995), arXiv:hep-ph/9505203.
- [36] M. Spira, (1995), hep-ph/9510347.
- [37] K. Arnold *et al.*, Comput. Phys. Commun. **180**, 1661 (2009), arXiv:0811.4559.
- [38] D0, V. M. Abazov *et al.*, (2010), arXiv:1002.4594.
- [39] T. Kluge, K. Rabbertz, and M. Wobisch, (2006), arXiv:hep-ph/0609285.
- [40] H.-L. Lai *et al.*, (2010), arXiv:1004.4624.
- [41] <http://hep.pa.msu.edu/cteq/public/ct10.html>.